DESIR Progress Report 2012

SPIRAL2 week, Caen, 23-27 January 2012

The work on DESIR in the last few months was mainly around the following topics:

- DESIR infrastructure to define in more detail the DESIR building and the beam transfer tunnels
- SHIRaC cooler
- High-resolution separator HRS
- DESIR transport beam lines
- Experimental equipment
- DESIR Collaboration Agreement

DESIR infrastructure:

A lot of work has been done again this past year to improve and complete the EQUIPEX call to get financing for the DESIR infrastructure. The funding request was in total about 15 M€. We are very happy that a funding of 9 M€ was granted by the French Ministry of Higher Education and Research. Although this does not cover the funds necessary to build DESIR in its full size, it nevertheless ensures the construction of DESIR at least in a basic version. Presently we are working on a reduced version of DESIR to see to which extent the costs for the DESIR construction can be reduced knowing that basically nothing can be gained on the transfer beam lines as the distance between the buildings will most likely not change, the only option with this respect being to equip at the beginning only one or two of the three transfer tunnels. Therefore, the main cost reduction has to come probably from a smaller DESIR hall (basement and experimental hall). However, we are looking also into complementary funding possibilities.

In addition, the layout of the DESIR hall has been improved to fulfil user requests and to thus optimise the installation of equipment in DESIR. Figure 1 shows the current installation plan of the experimental equipment of DESIR. This installation is to some extent still schematic and will be optimised in the future depending on the setups ready for installation, when the buildings will be delivered, on the size or the DESIR hall etc.

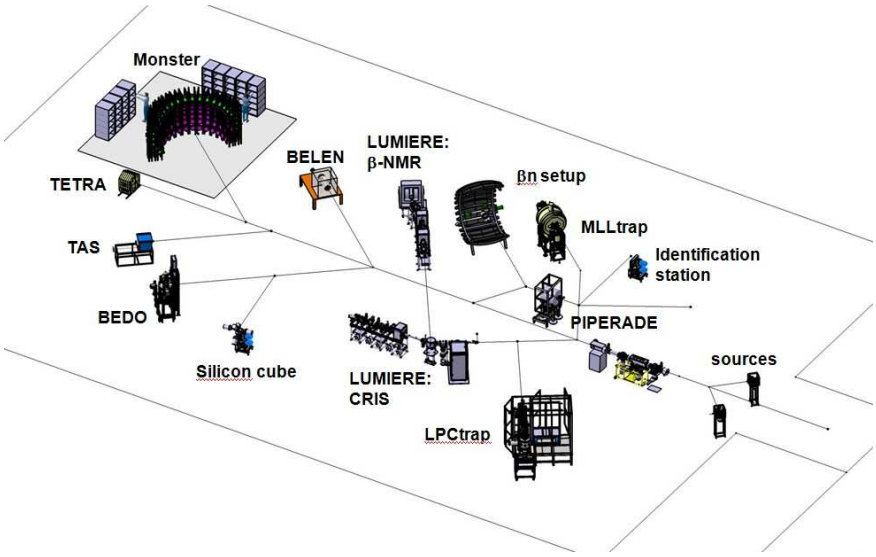

Figure 1: Layout of the DESIR hall with the experimental equipment installed as proposed by the future DESIR users.

Finally, in the frame work of the detailed design study of SPIRAL2 Phase 2 the power consumption, heat dissipation, cooling water and liquid helium needs have been defined in more detail for most of the experimental equipment.

The beam cooler SHIRaC:

Since the last status report in September 2011, several measurements have been performed, some of them are within the specifications, some are outside the specifications.

- the transmission is above 50% for 1µA Cs^{1+} beams
- the triplet can adapt the beam down to a width of about 1 mm in the horizontal plane
- the purity after the cooler is 100% with caesium ions; still further investigations are necessary with species other than alkali elements.

Preliminary results for the emittance and energy spread at high current are well above the requirements. It has to be noted that the setup used to measure both is not optimum. Very low emittances are difficult to measure with the present setup (pepperpot). The preliminary results show emittances in the range of 5-7 π.mm.mrad compared to the 1 mm*mrad required. The energy spread is even worse with measurements in the range of 10 eV. These values can be lowered to the specification range (1 π.mm.mrad, 1 eV) by lowering the RF voltage, but in this configuration the transmission drops to 20-25 %. Further investigations and studies of the extraction zone are underway.

The design of the cooler for nuclear environment has progressed (figure 2) and the final cooler should be validated by spring during the cooler review with the SPIRAL2 group.

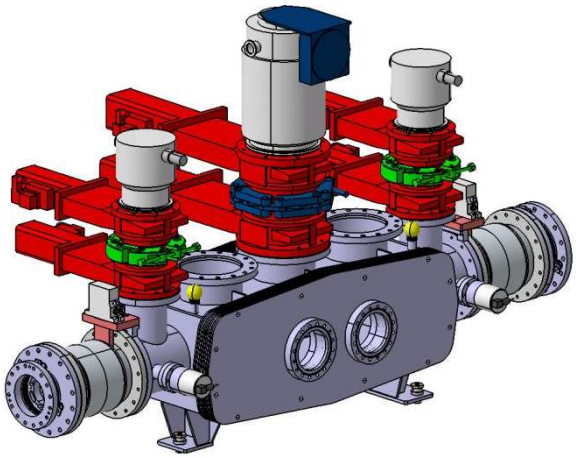

Figure 2: Design of the cooler SHIRaC adapted to the nuclear environment in which it is supposed to run.

The high-resolution separator HRS:

The DESIR-HRS is a two-stage magnetic dipole mass separator designed for the purification of high-intensity beams of exotic nuclides, located in the production building of SPIRAL2. The design for the DESIR-HRS is now essentially complete. It consists of two 90-degree magnetic dipoles (D) with 36-degree entrance and exit angles, matching quadrupoles (MQ), focusing sextupoles (FS), focusing quadrupoles (FQ), and one multipole (M) with the configuration QQSQDMDQSQQ. Mirror symmetry is imposed with respect to the mid-plane to minimize

aberrations. Focusing and corrective elements are all electrostatic and thus settings are independent of mass. To inject the purified beam into the 1+ line of the production building, a transport section is placed at the exit of the HRS, consisting of two quadrupole doublets and two 45-degree electrostatic benders.

A DESIR-HRS workshop was held at the CENBG, Bordeaux on November 17-18 2011, where mass separator experts discussed the optical characteristics and the mechanical design of the HRS. The proposed symmetric, two-stage solution has been unanimously validated as the best solution. Details on the design and performances are given in the technical design report in appendix 1, which constitutes a DESIR milestone within the SPIRAL2 PP.

In the near future, the detailed mechanical design and its installation will be completed. In the course of this year, the dipoles of the HRS will be ordered. 400 k€ from the CPER Basse Normandie are available for 2012. Full specifications and detailed mechanical designs of the magnets will be provided in the tender document that will be sent to possible manufacturers. Other elements of the HRS will be manufactured either at CENBG or by outside companies supervised by CENBG. An assembly hall was recently completed at CENBG where the HRS will be mounted for testing. The ion source and the cooler and buncher required for the tests will be shared with the PIPERADE project financed by the French ANR funding agency. The installation at CENBG is foreseen during 2013, tests (transmission, resolution) during 2014 and the transfer to GANIL is envisioned for 2015.

The beam transport lines:

Work on the beam transport lines was mainly conducted by IPN Orsay, in collaboration with VINCA institute. The main aim was to test whether the basic assumptions for the beam transport to DESIR are realistic. Therefore, calculations have been performed from the SPIRAL2 production building to the entrance of the DESIR hall. The 70 meters beam line as simulated with the TraceWin code is shown in figure 3.

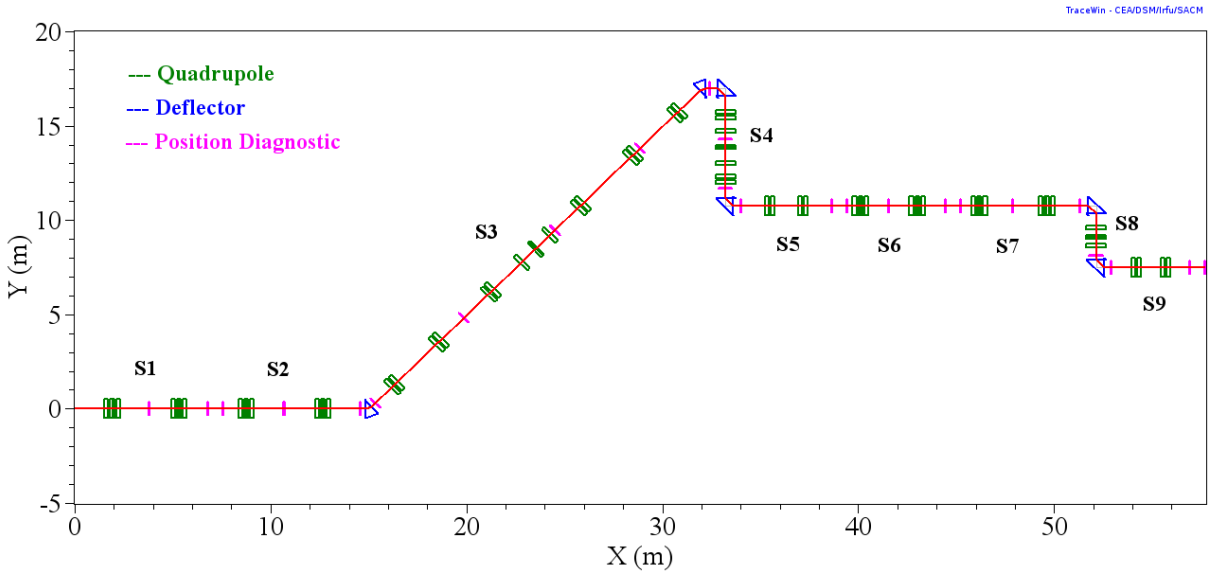

Figure 3: Scheme of the DESIR beam transport line from the SPIRAL2 production building to the entrance of the DESIR hall using the TraceWin code. Only qudrupoles, deflectors and diagnostics are reported.

The simulations showed that the beam lines can easily be fit into the building constraints. An error analysis showed that all expected transport uncertainties, due to an offset in beam position, beam angles at the starting point and other optical problems can be corrected with the steerers foreseen. However, the optimum positions of these elements still have to be determined.

A report on the DESIR beam transport is one of milestone for DESIR in the frame work of SPIRAL2PP. This report which is a preliminary report on the design of the beam line from the SPIRAL2 production building to the DESIR hall is attached to this report as appendix 2.

Experimental equipment:

Significant progress was also achieved for the different experimental setups. The principle of the CRIS (Collinear Resonant Ionization laser Spectroscopy) was successfully tested at ISOLDE with offline runs and a first online run on Francium isotopes. The CRIS beam line as installed at ISOLDE is shown in figure 4. As can be seen from figure 1, a similar beam line is foreseen at DESIR.

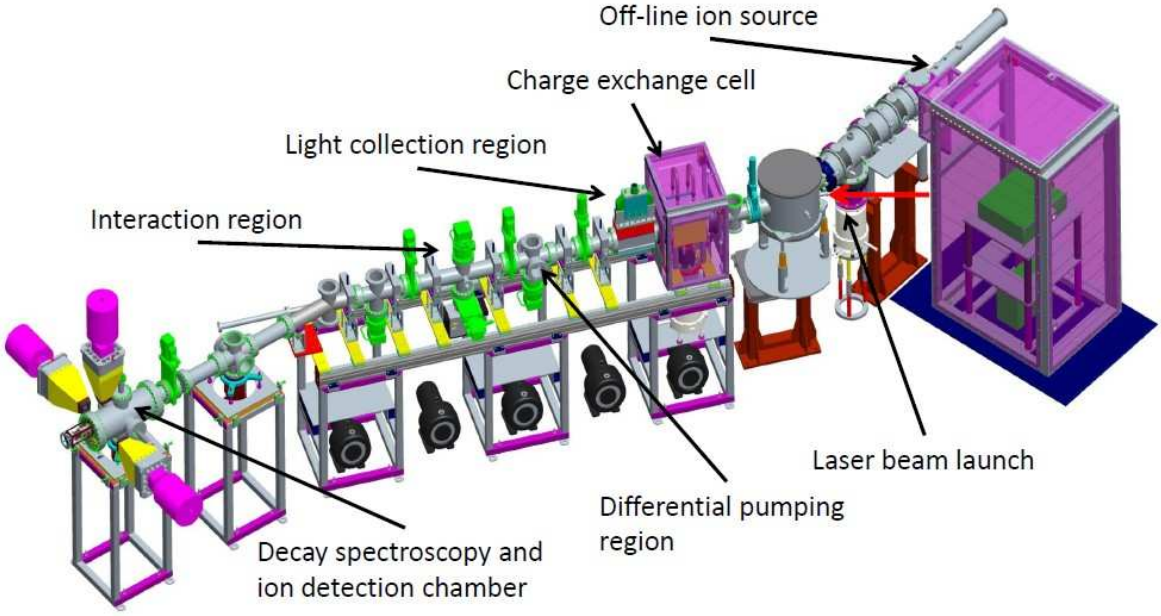

Figure 4: CRIS beam line as installed at ISOLDE. This beam line was recently commissioned with offline tests and a first online test with Francium isotopes.

Work on PIPERADE, the DESIR beam purification and preparation double Penning trap, has also started. Preliminary tests of the separation principle have started at MPI Heidelberg in the frame work of a CENBG-MPI-CSNSM-GANIL collaboration and two PhD students have been employed.

Similarly, constant progress has been made with the MLLtrap. A report on “Development and tests of the MLLtrap” is one of the milestones for DESIR within SPIRAL2PP. This report is attached to the present document as appendix 3.

DESIR Collaboration Agreement

Over the last year, we have worked out a DESIR Collaboration Agreement (DECA) on the installation of equipment in the DESIR hall. This agreement defines the rules and responsibilities of the different partners, sets up the management structure of DESIR and gives details about the financial and man-power input of the different partner. It runs until the installation of DESIR is completed and will then be replaced by and MoU concerning the long-term running of the facility. It will also be complemented by a Consortium Agreement for the construction of the DESIR infrastructure in the frame work of the EQUIPEX funding of DESIR.

This DECA will be signed during the SPIRAL2 week by the 14 partners. It is considered an important milestone for the DESIR collaboration, as it clearly defines the partners, their rights and duties and it will strengthen the collaboration. It is a deliverable of the DESIR collaboration for the SPIRAL2 Preparatory Phase contract with the EU. It is attached to this document as Appendix 4.

Conclusions

Steady progress has been achieved for the DESIR facility. The DESIR infrastructure design has been continued, as well as the tests of the prototype of the SHIRaC cooler, the technical design of the HRS has been completed and different parts of the DESIR experimental equipment were tested and improved.

In the frame work of SPIRAL2PP, three reports - on development and tests of the MLLtrap, on the DESIR transfer beam lines, and on the DESIR high-resolution separator HRS – were defined as milestones for DESIR. These reports have been completed and are attached to this document.

The selection of the DESIR project by the EQUIPEX program in December 2011 will allow financing at the level of 9 M€ part of the facility construction and operation from 2012 to 2020.

The signature of the DECA, the DESIR Collaboration Agreement, is an important step for the DESIR collaboration and defines the frame work of the installation of experimental equipment in DESIR.

APPENDIX 1

DESIR high-resolution separator HRS

Title: **Technical report for the DESIR High-Resolution Separator (DESIR-HRS)**

Authors: T. Kurtukian-Nieto[1], R. Baartman[2], T. Bataille[1], B. Blank[1], T. Chiron[1], C. Davids[3], F.Delalee[1], M. Duval[4], D. Lunney[5], F. Méot[6], L. Serani[1], M.-H. Stodel[4], F. Varenne[4], H. Weick[7]
([1] CENBG, [2] TRIUMF, [3] ANL, [4] GANIL, [5] CSNSM Orsay, [6] BNL, [7] GSI)

The DESIR-HRS is required to provide mass-purified beams of exotic nuclides from the SPIRAL2 production building. A two-stage magnetic dipole mass separator has been designed for 60-keV beams up to mass number 300 (rigidity of 0.61 T-m). The mass dispersion allows a maximal resolving power $m/\Delta m$ of 31000 for a 1π-mm-mrad beam emittance. The small emittance is achieved using a buffer-gas-filled, linear quadrupole ion guide in front of the separator.

Introduction

The DESIR (Désintégration, Excitation et Stockage d'Ions Radioactifs) facility is part of the new equipment necessary for exploitation of the radioactive beams produced by SPIRAL2. DESIR includes a laboratory equipped with beam lines for low-energy experiments that can receive nuclides from the SPIRAL1, SPIRAL2 and S3 installations at GANIL. DESIR also includes an important instrument for beam purification, located in the production building of SPIRAL2: a high-resolution mass separator (HRS) for high-intensity beams (see Figure 1).

The DESIR-HRS includes two dispersive magnetic dipoles, preceded by a beam-cooling device [SHIRAC] that provides low-emittance beams for higher mass separation. Resolving power depends on magnetic dispersion and inversely on beam emittance. The concept of reducing the beam emittance for mass separation, originally conceived for the ISOLDE facility [ISOLDE] was elaborated in the context of the EURISOL Design Study [EURISOL].

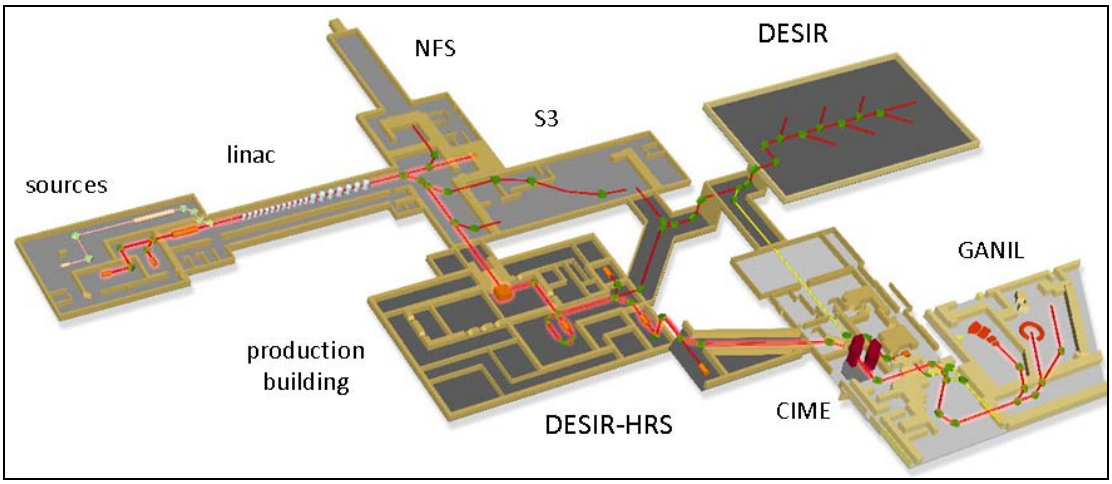

Figure 1: *Schematic layout of the entire GANIL facility including SPIRAL1, SPIRAL2, and DESIR.*

The beam cooler will provide the small emittance needed for the DESIR-HRS to achieve its design goal of a resolving power of $m/\Delta m$ = 20000. As shown in Figure 2, a resolving power of 1000-2000 is enough to separate light exotic nuclei. However, for the medium-mass nuclei produced by SPIRAL2, a resolution well in excess of 10000 is needed.

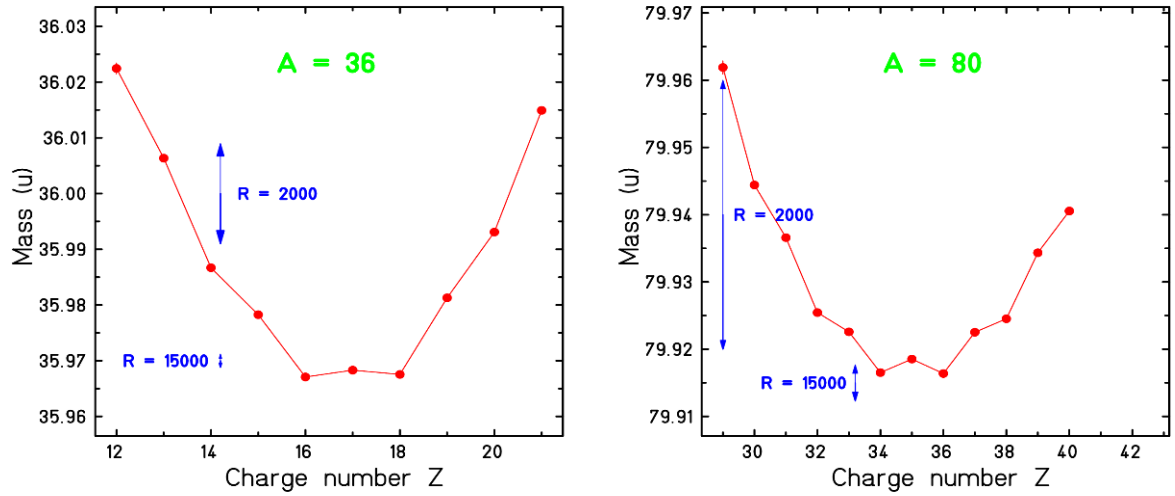

Figure 2: *Isobaric masses of A=36 (left) and A=80 (right) nuclides. The arrows indicate different mass resolving powers.*

SPIRAL2 is not the first radioactive beam installation to attempt the construction of an HRS. In fact, there is little success in obtaining high resolving power with magnetic dipoles, despite extensive efforts. The ISAC facility at TRIUMF recovered the mass separator from Chalk River Laboratories when the TASCC facility there was closed. At Chalk River, the separator achieved a resolving power of 20 000 using collimated (0.1 mm) stable beams and 5 700 for exotic species [CRNL]. ISAC typically operates with a lower resolving power, for ease of operation. The other example is the ISOLDE HRS, originally designed for 30 000, which routinely achieves only 4 500, although a different configuration is now used [ISOLDE]. The more recently designed separator for the CARIBU project [DAV08] has not yet achieved its design goal of 20 000, but tests are underway. A workshop was held at the CENBG (Bordeaux) where mass separator experts were able to discuss different approaches and the most plausible solution was unanimously a symmetric, two-stage solution.

The proposed design (see Fig. 3) consists of two 90-degree magnetic dipoles (D) with 36-degree entrance and exit angles, matching quadrupoles (MQ), focusing sextupoles (FS), focusing quadrupoles (FQ), and one multipole (M) with the configuration QQSQDMDQSQQ. Mirror symmetry is imposed with respect to the mid-plane to minimize aberrations. Focusing and corrective elements are all electrostatic and thus settings are independent of mass. To inject the purified beam into the 1+ line of the production building, a transport section is placed at the exit of the HRS, consisting of two quadrupole doublets and two 45-degree electrostatic benders. The detailed calculations are discussed in the following sections.

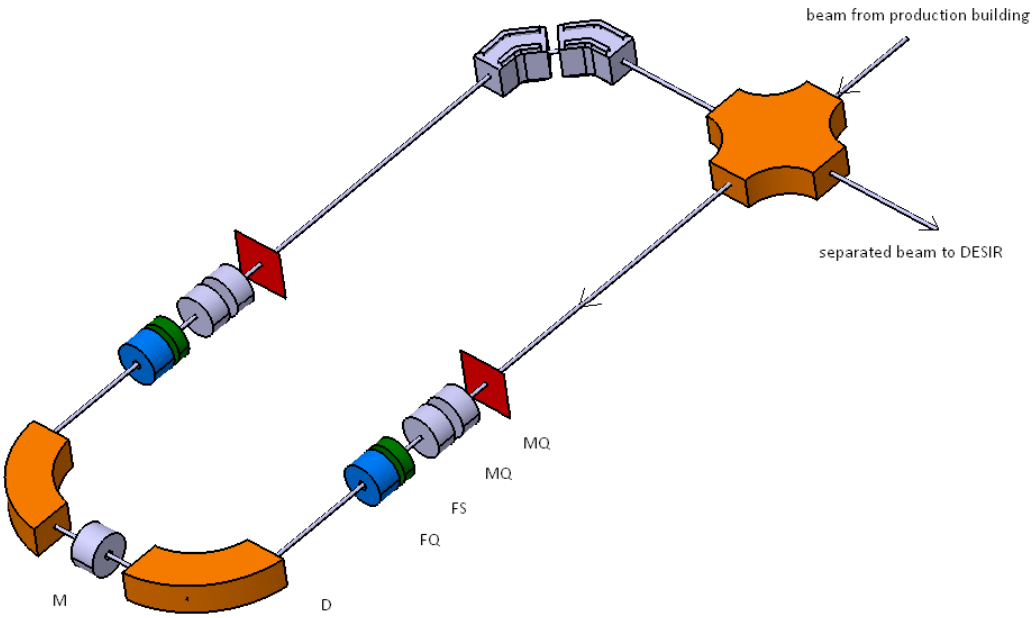

Figure 3: *Optical layout of the DESIR-HRS. Separation is performed using two 90-degree magnetic dipoles (D) with 36-degree entrance and exit angles. Mirror symmetry is imposed with respect to the mid-plane to minimize aberrations. The entrance beam optics was designed using matching quadrupoles (MQ), a focusing sextupole (FS), and a focusing quadrupole (FQ). A multipole (M) is placed at the mid-plane, between the two magnetic dipoles. The overall configuration is: MQ-MQ-FS-FQ-D-M-D-FQ-FS-MQ-MQ. After the second focal plane, two quadrupole doublets (not shown) and two electrical benders of 45° allow the system to match the 1+ line of SPIRAL2.*

DESIGN OF THE MAGNETIC DIPOLES

The magnetic dipoles are the most costly single elements of the DESIR-HRS. Simulations have been performed by the magnet group at GANIL using the following specifications:

Parameters for the Dipoles			
Characteristic	Value	Units	Comments
$B\rho_{max}$	0.45	Tesla-meters	
Vertical gap	0.07	meters	
Homogeneous region	0.40	meters	Transverse homogeneity optimized for 0.3 m, but still reasonable for 0.4 m
Curvature	0.85	meters	Beam bending radius
Angle	90	degrees	Beam bending angle
Pole face angles	36	degrees	Input and output

Simulations were made using the magneto-static module of the software OPERA. The dipoles have been designed in order to obtain the best homogeneity in the central zone, where most of the particles are transmitted. The field simulation and obtained homogeneity are shown in Fig. 4.

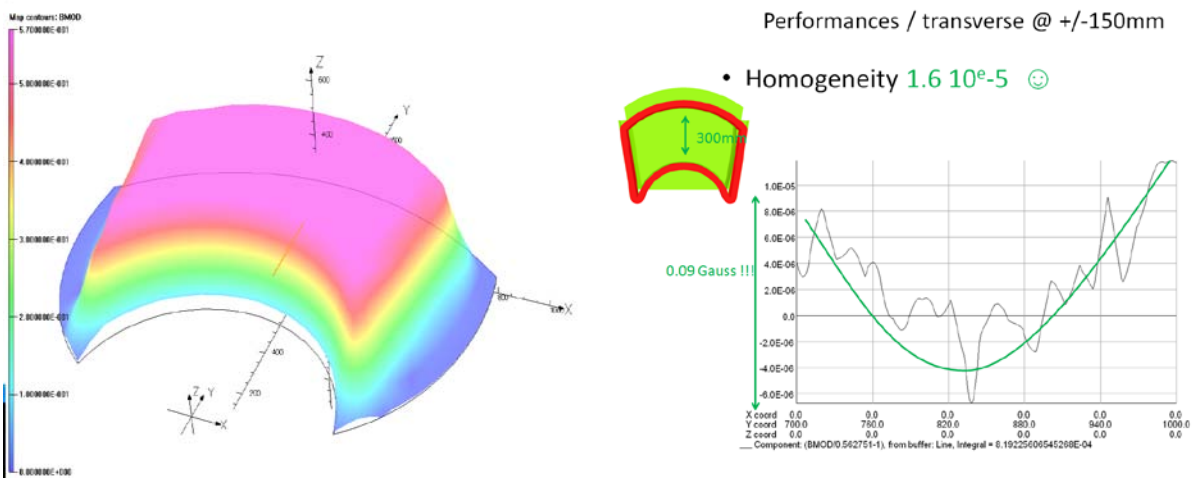

Figure 4*: Dipole field map and central homogeneity as calculated using TOSCA.*

The central (middle deviation) homogeneity obtained on the simulations represents the best we could achieve with the specifications, but it might be difficult to obtain over whole range of $B\rho$. At $B\rho_{min}$, the homogeneity is around 1.1×10^{-4}. The sensitivity of the homogeneity to several dimensions of the magnet has been evaluated with simulations to allow for deviations due to fabrication. The simulation field maps have been used in several beam optics calculations, in order to validate the design.

Design characteristics of the dipole			
Characteristic	Value	Units	Comments
Iron mass	6000	kg	Chosen to reduce saturation and variation of magnetic length
Copper mass	390	kg	
cooling circuits	6		per dipole
Cooling circuit length	74	m	per circuit
Conductor	8/8/4.5	mm	Width/height/hole diameter for the main power supply
Turns	96		
Current	210	A	maximum
Power supply	17	kW	not including correction coils

Note that this design is adapted to the $B\rho_{max}$, and is not suitable for higher magnetic rigidity, but the coil can be shared with a design adapted to $B\rho_{max}$= 0.6 T-m.

The geometrical characteristics of the dipole chosen to obtain good transversal homogeneity are shown in Fig. 5. The detailed mechanical design of the magnets can be seen in the figures. The full specifications will be described in the tender document that will be sent to prospective manufacturers.

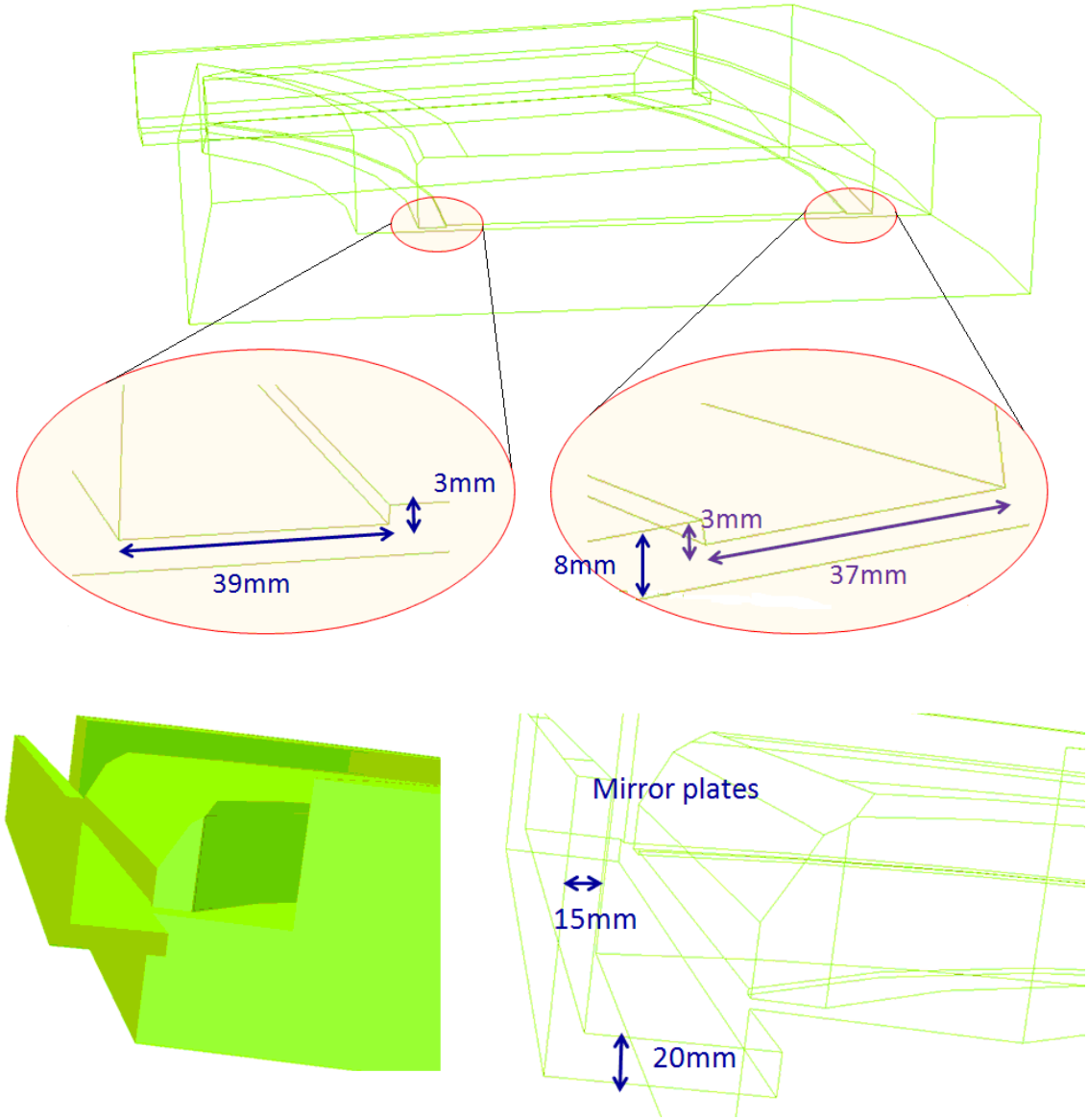

Figure 5: *Details of the dipole magnet geometry, including dimensions. This is just to show that the design of the magnets has reached an advanced stage. The full description of the geometry will be given in the tender document sent to prospective manufacturers. (top) the shim coil guide details and (bottom) the details for the fringe field end shielding.*

ION OPTICS, TRANSFER MATRIX AND BEAM ENVELOPES

The ion-optical code COSY INFINITY [Ber90] was used as a base of calculations. The phase space dimensionality used was 2, being the *x-a* (horizontal) as well as *y-b* (vertical) motion computed. δm is calculated as a parameter. Thus all calculations are performed in the following scaled coordinates:

$$[1] = x;\ [2] = a = p_x/p_0;\ [3] = y;\ [4] = b = p_y/p_0;\ [5] = \delta m = (m-m_0)/m_0$$

The beam enters the HRS by a 1 mm^2 slit, with a maximal angular dispersion of ±10 mrad and passes through the first quadrupole doublet, which consists of a pair of quadrupoles of opposite polarity. This matching section produces a ribbon-shaped beam. The next quadrupole makes the beam to diverge in radial (x-direction) and to converge in vertical. The divergent beam envelope is designed to occupy the entire dipole magnet acceptance to maximize mass dispersion. The combined effect of the entrance and exit angles of the dipoles produces a parallel beam in the radial direction. The focusing condition at the mid-plane is (a,a) = (y,b) = (b,y) = 0: point-to-parallel in x, and point-to-point/parallel-to-parallel in y. The symmetric half of the separator allows refocussing the beam to a 1 mm^2 envelope and making the mass selection with the slits placed at the image focal plane.

After the HRS, an ensemble of two quadrupole doublets and two 45° electrical benders allow to transport the beam until the compensation point of the 1+ line, homothetically (meaning: *different emittance but with the same relative orientation of the components*) at 80 π-mm-mrad. At this point the beam is considered as emitted from a minimum envelope of marginal dimensions of ± 2.25 mm horizontally and ± 7.45 mm vertically. The first order transfer matrix of at the image focal plane is:

	x_f	a_f	y_f	b_f					
$\frac{\partial}{x_0}$	-1.000	-3.650	0.000	0.000					
$\frac{\partial}{a_0}$	-0.397E-05	-1.000	0.000	0.000	$\frac{\partial}{b_0}$	0.000	0.000	-0.601E-06	1.000028
$\frac{\partial}{y_0}$	0.000	0.000	1.000	0.5013E-04	$\frac{\partial}{\delta m}$	-31.32	-57.16	0.000	0.000

The calculated beam line envelopes are shown in the following figures. The following table summarizes the calculated parameters for the electrostatic elements.

Parameters of electrostatic elements			
Element	Value (kV)	Element	Value (kV)
MQ1	-6.7E-01	M- Decapole	-1.8E-02
MQ2	7.6E-01	M- Dodecapole	-8.4E-03
FQ1	-8.6E-01	FQ3	-5.275
FS1	7.0E-02	FQ4	1.873
M- Sextupole	-7.6E-01	FQ5	0.361
M- Octupole	-6.0E-02	FQ6	-0.650

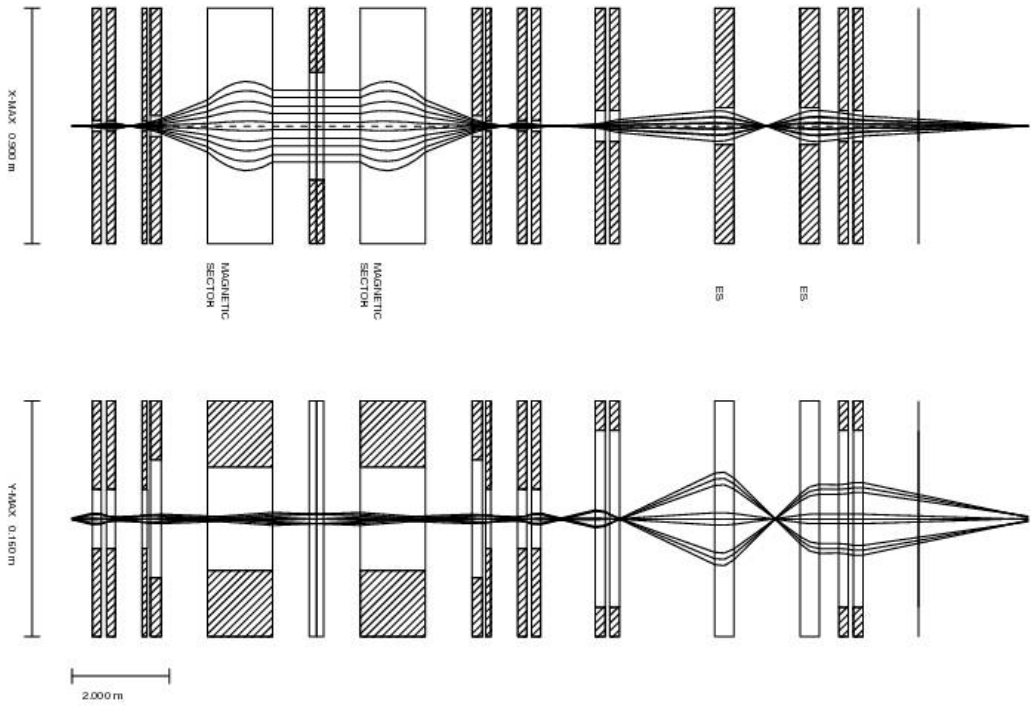

Figure 6: *Beam envelopes of the HRS in the x-(dispersive) and y-(non dispersive) planes calculated with the program* GICOSY [GICO]. *Please note the difference in the scale of both planes. The transport section for matching the 1+ line is included.*

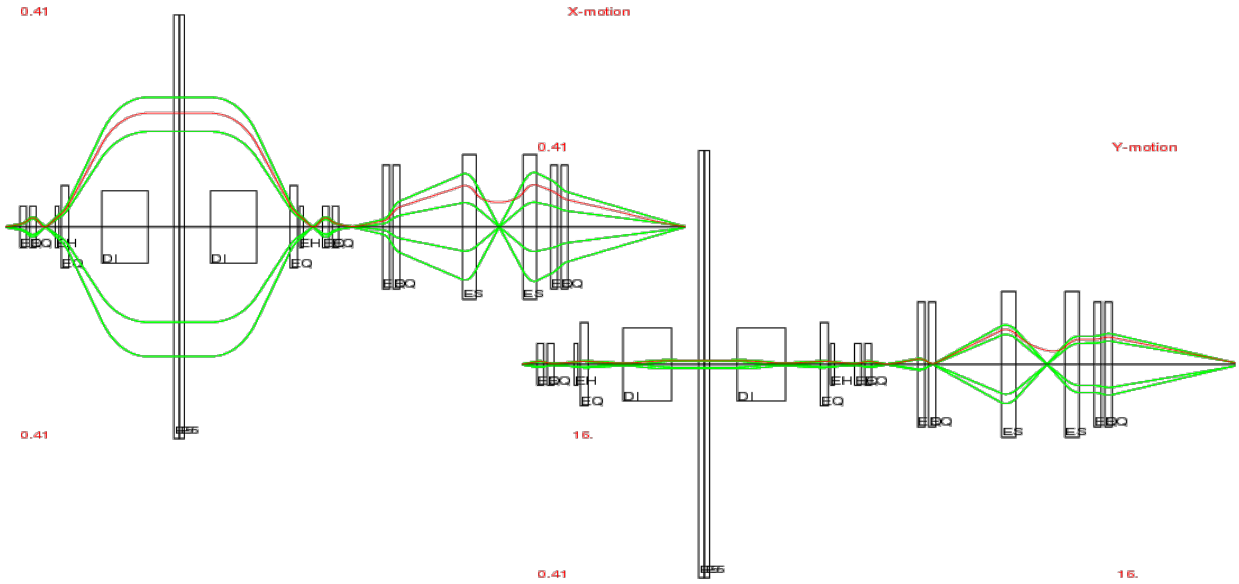

Figure 7: *Beam envelopes of the HRS in the x-(dispersive) and y-(non dispersive) planes calculated with COSY INFINITY.*

FIFTH-ORDER MONTE CARLO SIMULATION

In order to study the performance of the DESIR-HRS a Monte Carlo code has been developed. This code takes as input the transfer matrices as calculated from COSY INFINITY up to 5th order and propagates the beam through the different lattice elements. The output of the code are the initial and final phase spaces of the beam and the mass spectrum as calculated for the different masses introduced in the simulation. Fig. 8 shows the phase space diagrams after the separator assuming perfect geometrical alignment and the focal plane mass spectrum.

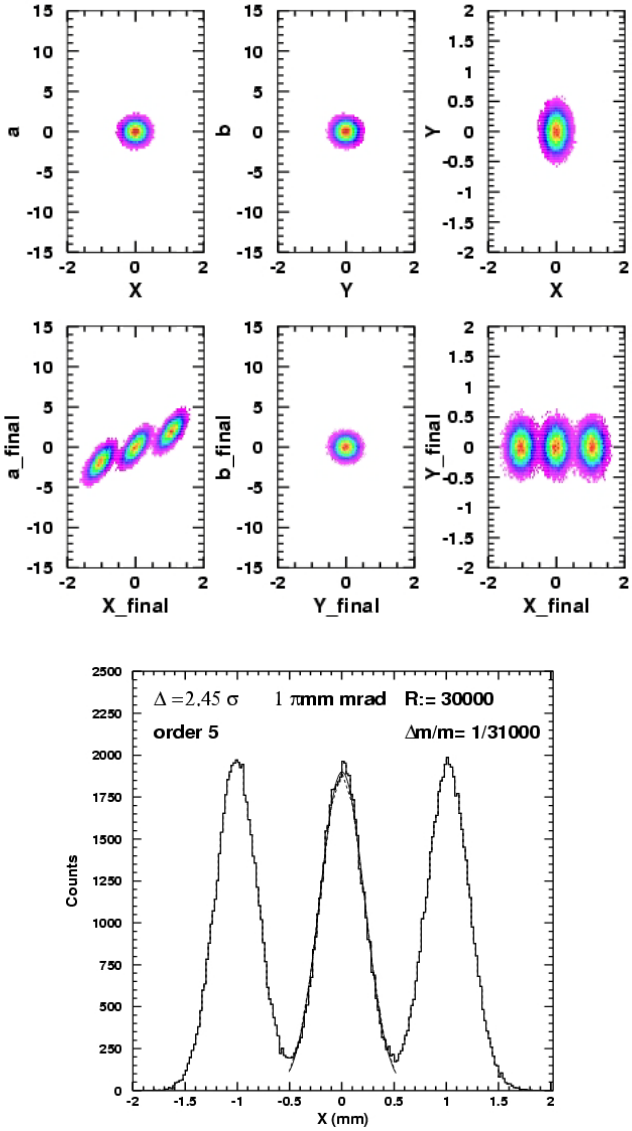

Figure 8: *Phase space calculated at 5th order for 50000 particules with mass deviations of -1/31000, 0, +1/31000. Top: Beam phase spaces at the exit of SHIRaC. Bottom: Phase spaces at the image focal point of the HRS. Mass spectrum calculated to 5th order for 50000 particules with mass deviations of -1/31000, 0, +1/31000.*

In order to simulate more realistic conditions reflecting manufacturing defects and optical element mis-alignment, the simulations were redone by varying the beam positions for each element according the to following table:

Module	ΔX(mm)	ΔY(mm)	Δθ(°)
1	+0.1	-0.1	-0.2
2	-0.1	+0.1	+0.2
3	-0.05	-0.05	-0.2
4	+0.1	+0.1	+0.2
5	-0.1	-0.1	-0.2
X-Offset (mm)	-0.09		
R	20477		

The corresponding phase space plots and mass spectrum are showing in Fig. 9.

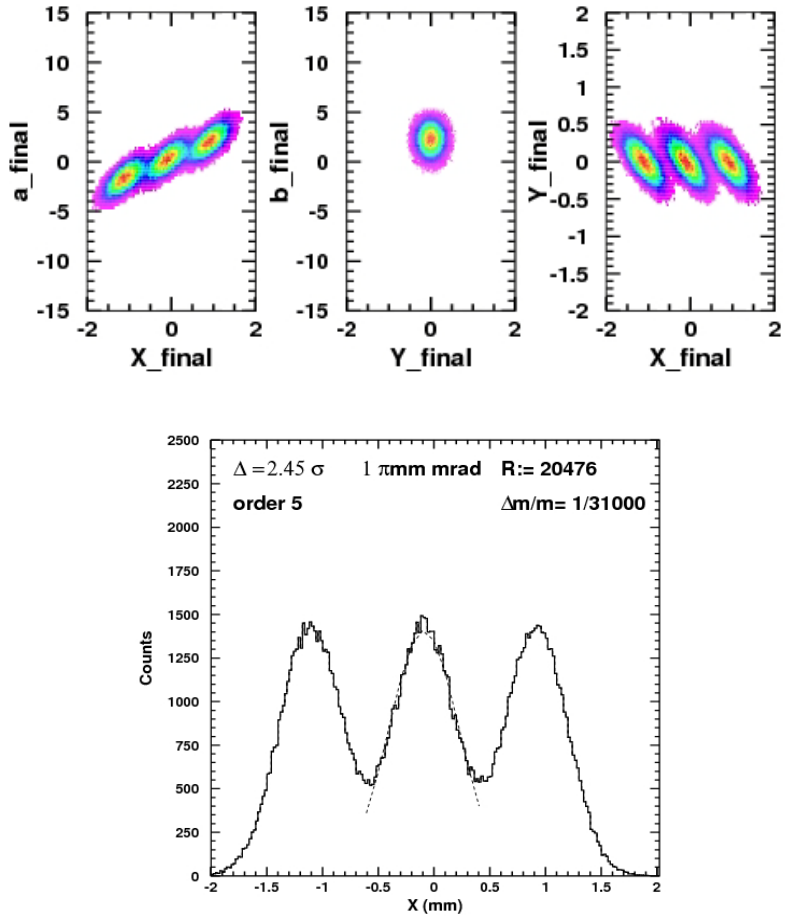

Figure 9: *Top: Phase space after the separator calculated using the maximal tolerance on the misalignment of the different optics modules, calculated at 5th order for 50000 particules with mass deviations of -1/31000, 0, +1/31000. Bottom: corresponding mass spectrum, showing the mass resolution decreased to ~20000.*

The above simulations assume that the neighboring isobaric masses are of equal intensity, which is rarely the case in reality. Another simulation was performed to take this into account. The following table lists isobaric beam intensities that are predicted by production simulations within the SPIRAL2 project.

Element	I (pps) [SPIRAL2]	Δm/m [Ame2003]	Δx (mm)
Cd	$3.5\,10^{2}$	$-2.1\,10^{-4}$	+6.5
In	$1\,10^{6}$	$-1.2\,10^{-4}$	3.6
Sn	$9.5\,10^{8}$	0	0
Sb	$1.9\,10^{9}$	$+2.5\,10^{-5}$	-0.8
Te	$6.6\,10^{9}$	$+7.0\,10^{-5}$	-2.2
Xe	$7.4\,10^{10}$	$+1.0\,10^{-4}$	-3.2
Ba	$2.2\,10^{1}$	$+9.7\,10^{-5}$	-3.1

The resulting mass distributions are shown in Fig. 10.

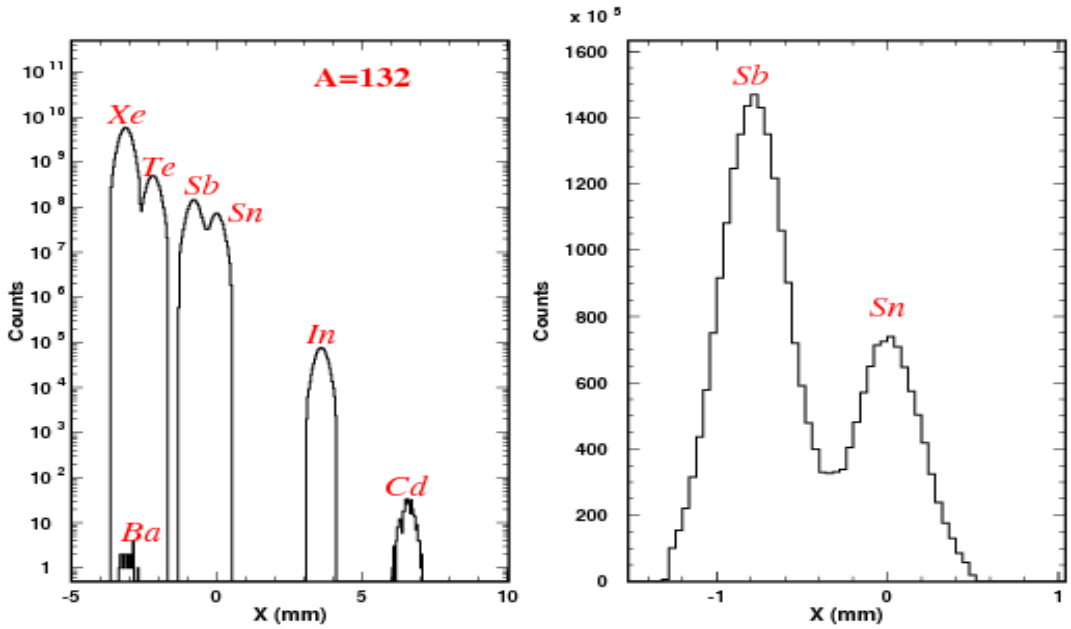

Figure 10: *Left: Mass spectrum calculated at 5th order considering all A=132 elements produced from n-induced fission 50-kW deuteron beam, a 280-g (3.5-g/cm^3) UCx target, with the separator tuned to center ^{132}Sn. Intensities are taken from [SPIRAL2]. Right: Zoom of the mass spectrum in linear scale. The colored zone indicates slits which, if placed at ± 0.5mm, the transmission of ^{132}Sn is 97% with a 13.3% contamination of ^{132}Sb. If the slits are closed to ±0.25 mm the contamination is eliminated but the transmission of ^{132}Sn is reduced to 61%.*

MODULE INTEGRATION

For safety requirements of the SPIRAL2 project, the DESIR-HRS is divided into seven modules, each of which is separated by gate valves, as shown in Figure 11. Each module can be isolated and removed independently in case of contamination. The seven modules essentially follow the DESIR-HRS optics design: (1) injection quad-quad and hex-quad lenses; (2) first magnetic dipole; (3) electrostatic multipole; (4) second magnetic dipole; (5) extraction quad-quad and hex-quad lenses; (6) first 45-degree bender; (7) second 45-degree bender.

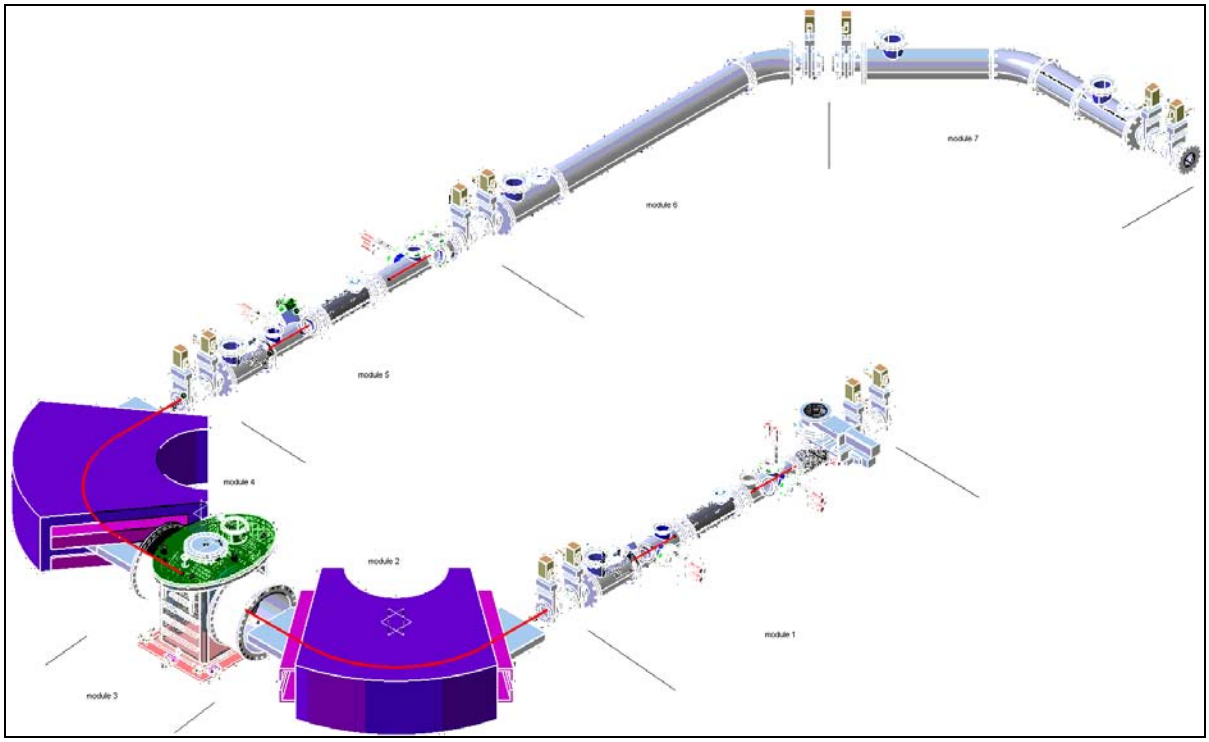

Figure 11: *Modular structure of the DESIR-HRS required by the SPIRAL2 safety authorities.*

Summary and outlook:

The design for the DESIR High Resolution Separator (DESIR-HRS) is now essentially complete. The design takes into account past experience from separator experts at radioactive beam installations worldwide. Several ion optics codes have been used to verify coherence of the optical solutions and to cross check the predicted performance. The different codes

include: COSY INFINITY, TRANSPORT, GALOP, ZGOUBY and GICOSY, with calculations up to 5th order.

The design of the HRS relies on a strong optical focussing for a wide illumination of small dipoles in order to minimize the size of the separator. This optical condition makes the system more sensitive to the fringe field effects and to the homogeneity of the dipole field. A correct simulation of such effects is important in order to predict the necessary corrections. Simulations using TOSCA and SIMION8 show that this will be feasible. The design for the magnetic dipoles also includes the possibility of easily changing magnetic edges to refine the minimization of aberrations.

Considering the maximal tolerance on the misalignment of the different modules as verified with the land surveyor of the project, a resolution of ~20 000 can be achieved for a beam emittance of 1 π-mm-mrad at 60 keV.

References

[DAV08] C. Davids, D. Peterson, Nucl. Instr. Meth. Phys. Res. B **266** (2008) 4449 (2008).
[Ber90] M. Berz, Nucl. Instr. and Meth. A **298** (1990) 473
[EURISOL] Beam Preparation (chapter 6) in: The EURISOL Design Study Final Report, J. Cornell (ed.) GANIL press, 2009
[GICO] Program GICOSY, http://www-linux.gsi.de/~weick/gicosy/
[TRAN] PSI Graphic Transport Framework by U. Rohrer based on a CERN-SLAC-FERMILAB version by K.L. Brown et al.
[TURT] PSI Graphic Transport Framework by U. Rohrer based on a CERN-SLAC-FERMILAB version by K.L. Brown et al.
[CRNL] K.S. Sharma et al., Nuclear Instruments and Methods in Physics Research A275 (1989) 123-132; and H. Schmeing et al., Nuclear Instruments and Methods 186 (1981) 47-59
[ISOLDE] T.J. Giles et al., Nuclear Instruments and Methods in Physics Research B 204 (2003) 497–501
[SHIRAC] O. Gianfrancesco et al., Nuclear Instruments and Methods in Physics Research B 266 (2008) 4483-4487; F. Duval, Ph.D. thesis, U. Basse Normandie (2010)
[SPIRAL2] http://pro.ganil-spiral2.eu/spiral2/spiral2-beams/radioactive-ion-beams-of-spiral2/low-energy-desir-isol-rib-beams-available-for-the-day-1-spiral2-phase-2-experiments/intensities-from-n-induced-fission
[AME2003] G. Audi, A.H. Wapstra, C. Thibault, Nuclear Physics A 729 (2003) 337

APPENDIX 1: LATTICE CONFIGURATION FOR THE HRS

Module HRS			
Element	**Distance (mm)**	**Element**	**Distance (mm)**
Drift length L1 (diagnostics)	420	Drift length L6	750
Matching quadrupole MQ1 aperture = 40 mm	185	Dipole D2 ρ = 850 mm, θ = 90º β1=β2=36º Pole gap = 70 mm, width = 400 mm	1335
Drift length L2	100	Drift length D1 (Slits)	955
Matching quadrupole MQ2 aperture = 40 mm	185	Focus quadrupole FQ2 aperture = 80 mm	220
Drift length L3 (slits)	275	Drift length L5	60
Drift length L4 (diagnostics)	275	Focus sextupole FS2	110
Focus sextupole FS1	110	Drift length L4 (Diagnostics)	275
Drift length L5	60	Drift length L3 (Slits)	275
Focus quadrupole FQ1 aperture = 80 mm	220	Matching quadrupole MQ3 aperture = 40 mm	185
Drift length D1 (Slits)	955	Drift length L2	100
Dipole D1 ρ = 850 mm, θ = 90º β1=β2=36º Pole gap = 70 mm, width = 400 mm	1335	Matching quadrupole MQ4 aperture = 40 mm	185
Drift length L6	750	Drift length L1	420
Multipole M aperture = 410 mm,	300	Slits	

Beam Transport to the 1+ Line			
Element	**Distance (mm)**	**Element**	**Distance (mm)**
Drift length L7	850	EB ρ = 500 mm, θ = 45º, a = 140 mm	392.70
Quadrupole FQ3, a = 120 mm	200	Drift length L11	400
Drift length L8	100	Quadrupole FQ5 a = 120 mm	200
Quadrupole FQ4 a = 120 mm	200	Drift length L12	100
Drift length L9	1807.93	Quadrupole FQ6 a = 120 mm	200
EB ρ = 500 mm, θ = 45º, a = 140 mm	392.70	Drift length L12	1142.93
Drift length L10	1353.5	1+ Line Dipole	

Appendix 2: Performance study of the HRS using the code *Raytracing Turtle*

A set of simulations has also been performed for the DESIR-HRS by using the program *Raytracing Turtle* [TURT]. These versions were calculated and optimised using TRANSPORT [TRAN] to third order. Three isobars differing in mass by ±1/20000 were simulated. The transmission and the contamination to the central mass by the neighbourgs were calculated. All calculations were perfomed using a momentum dispersion of $\Delta p/p = \pm 0.0005$. The beam had 1mm width both in *x*- and *y*-directions. Two values for θ_{max} and φ_{max} were studied: ±2 and ±10 mrad, corresponding to the respective beam emittances: 1 π-mm-mrad and 5π-mm-mrad.

Figure 12 shows the spatial separation at the image focal point, for three isobars differning in mass by ±1/20000 for a beam emittance of 1π mm.mrad. Placing slits XY of 1mm^2, the transmision is of 86%. The cross-contamination is ~0%

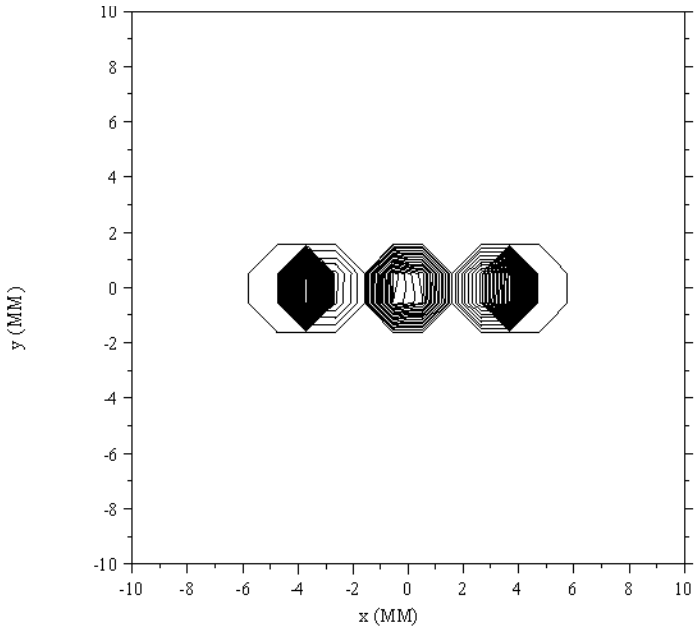

Figure 12: *Performance of the HRS as calculated with TURTLE for 1π mm.mrad, Δp/p=0.0005 and Δm/m=20000.*

For a beam emittance of 5π mm.mrad, we obtain a transmission of 45% at the focal point of the HRS and a cross-contamination of 1.5%.

APPENDIX 2

Beam line design report

SPIRAL2 – Phase 2

Beam dynamics study for the DESIR beam transfer section

EDMS reference: I-028784

Luc Perrot (perrot@ipno.in2p3.fr, +33 1 69 15 71 58)

12/01/2012

Introduction

In this report, we will present the results using the TraceWin [1] code for error calculations in the 1+ beam transfer line from the SPIRAL2 production building to the DESIR building.

After a presentation of the beam line, we introduce error sources and correction schemes. Position correctors (electrostatic steerers) in horizontal and vertical planes are employed for the beam alignment corrections.

I Line structure and beam specifications at the entrance

a Implementation

The considered beam lines are located in the SPIRAL2 production building and in its connection to the DESIR building (see Figure 1 and 2).

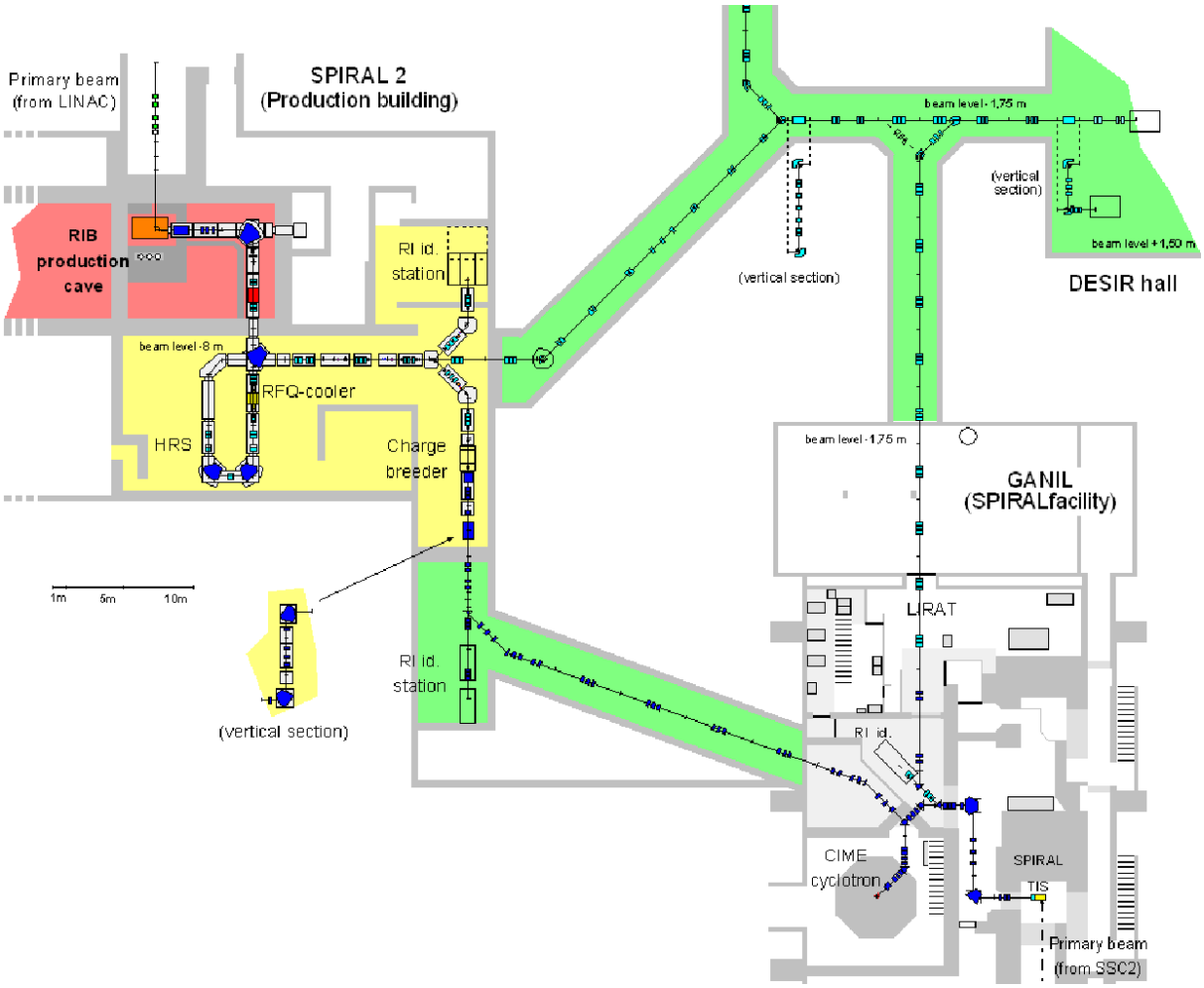

Figure 1: Overview of the SPIRAL2 phase 2 beam lines.

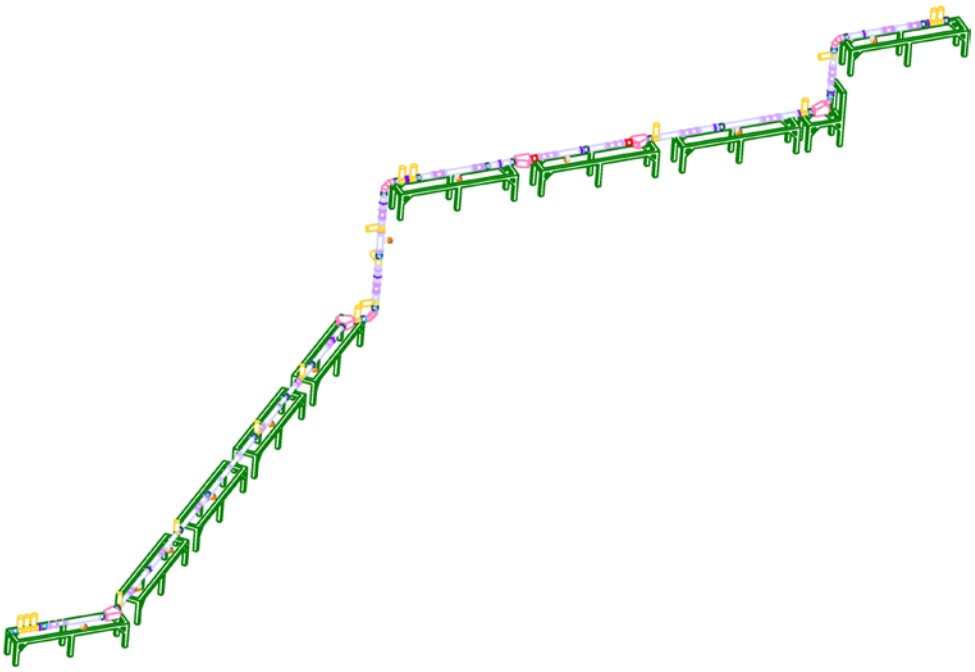

Figure 2: Beam line studied in the present work: Transfer from the 1+ adaptation point in the SPIRAL2 production building up to the adaptation point in the DESIR building.

b Structure of the line

The beam lines concerned by the present error calculations are presented in more details in the following scheme. It is extracted from the synoptic of the SPIRAL2 Phase 2 beam lines (version 3.5), see Figure 3.

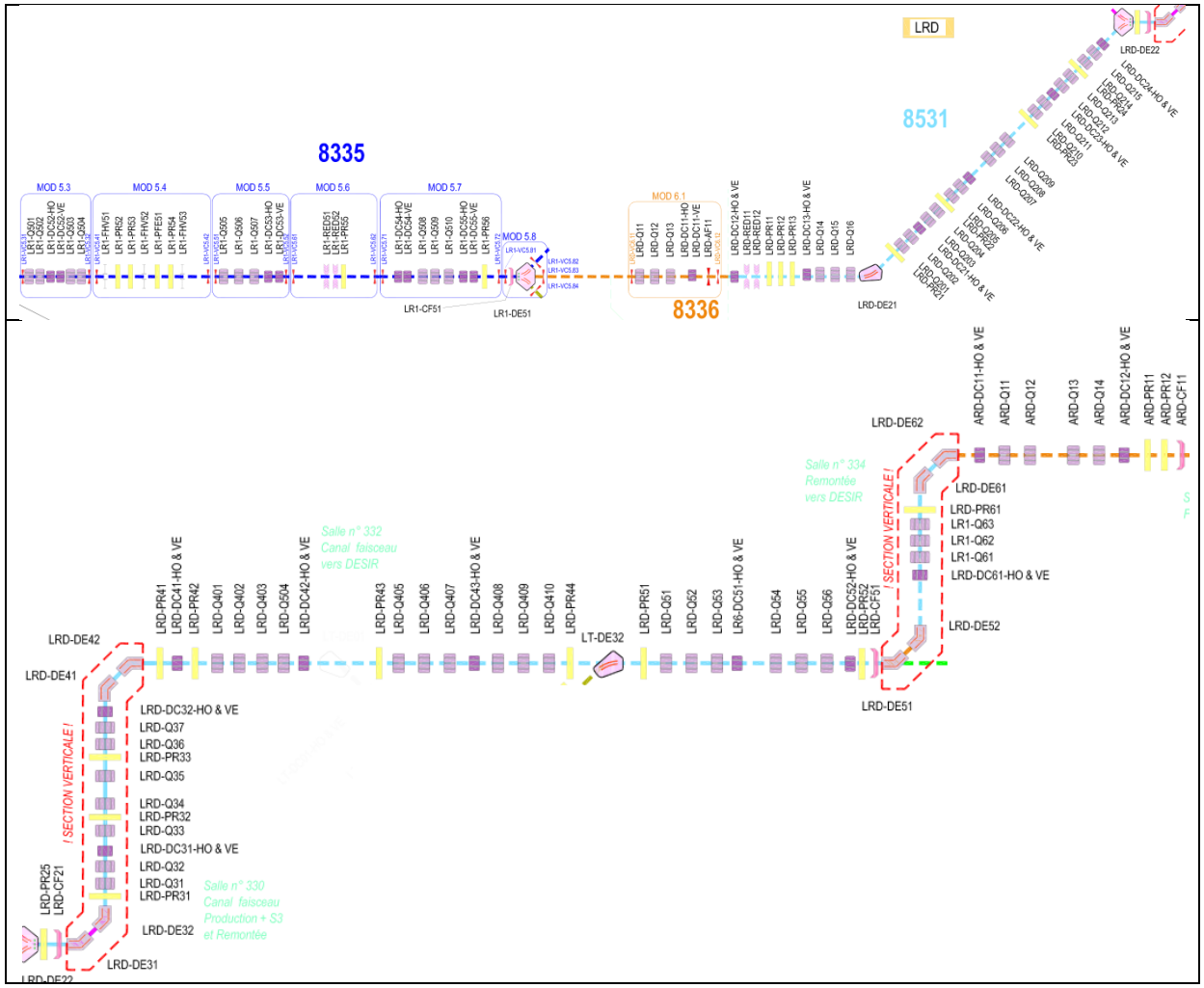

Figure 3 : Synoptics of the transfer beam line to the DESIR building.

After the magnetic dipole (from the 1+ production beam line or from the DESIR high-resolution separator HRS), beams are matched using two quadrupole doublets (Mod 5.3) in order to have a beam waist at the beginning of Mod 5.4. This beam waist is the starting point of the beam line studied in the following calculations (see ref. [2, 3]).

We continue by 2 quadrupole-triplet sections up a beam waist formed just before the LR1-DE51 electrostatic deflector (beam switching to the 1+ IBE station, to the 1+ - n+ charge breeder or to DESIR at 0°). This section is followed by 2 quadrupole-triplet sections up to the waist formed before the LRD-DE21 electrostatic deflector.

We follow by a long left-right deviation at 45° (15 electrostatic quadrupoles) joining the 1+ beam section coming from S3 and by a first vertical deviation (7 quadrupoles) which brings the beam line from -8 m to -1.75 m. After this vertical deviation, we have 3 sub-sections: a 4-quadrupole beam re-adaptation and 2 sextuplet sections. Next, we have the second vertical deviation which brings the beam line from -1.75 to +1.50 m which is followed by a 4-quadrupole beam re-adaptation section inside the DESIR building.

In the actual (December 2011) design, the structure is fixed up to Mod 6.1 (code PBS 8336). The distance from the waist in the Mod 5.4 up to the beam waist formed before LRD-DE21 is fixed. The location of the LR1-DE51 is also determined. Therefore, the two first quadrupole triplets are fixed and the available space is "known". The rest of the beam transport line is determined by the general skeleton but, inside each sub-section, the beam-optics implementation can be modified. The transfer line can be divided in 9 sub-sections (cf. Table 1 and Figure 4).

Section Number	Section Name	Section Length (mm)	Total Length (mm)
S1	First Sextuplet section	6800,0	6800,0
S2	Second Sextuplet section	7818,0	14618,0
S3	Left-Right deviation section	24807,6	39425,6
S4	First Vertical section (Δz=6.25mm)	7506,6	46932,2
S5	First re-adaptation section	4642,0	51574,2
S6	Third Sextuplet section	5800,0	57374,2
S7	4^{th} Sextuplet section	6880,0	64254,2
S8	Second vertical section (Δz=3.25m)	4506,6	68760,8
S9	Second re-adaptation section	4000,0	72760,8

Table 1: Sub-structure of the beam transfer line.

The quadrupole length is fixed to 200mm with an aperture pipe diameter arbitrary fixed to 100mm. The deflectors are chosen spherical with 45° or 90° deviation angle and a radius equal to 400mm.

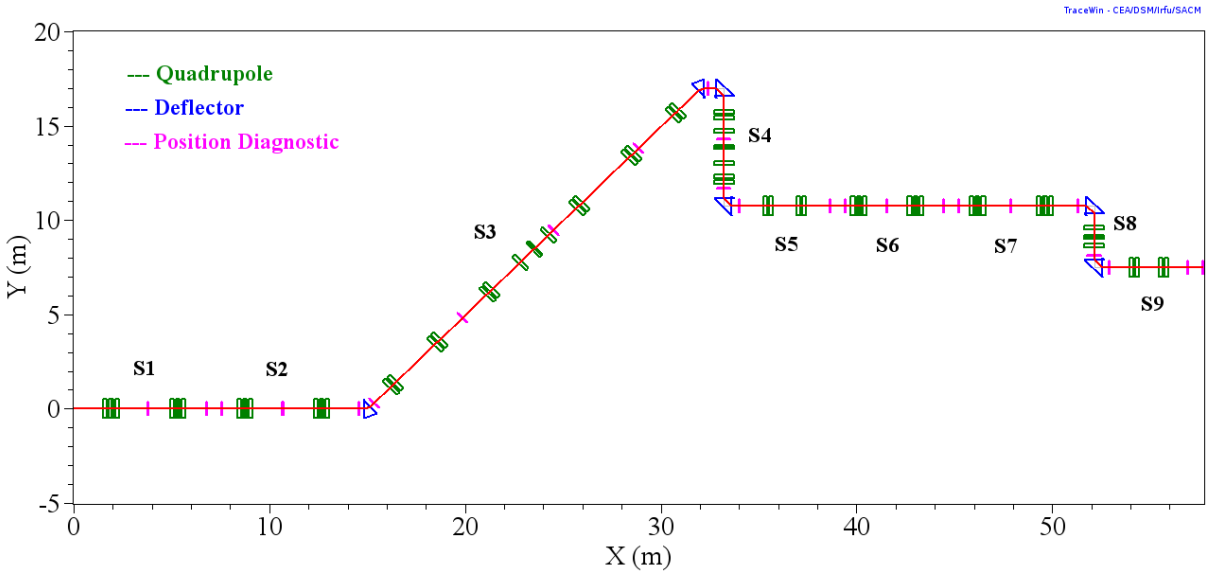

Figure 4 : Scheme of the line using the TraceWin code. The steerers are not reported.

Table 2 gives the details of the beam line as it was studied for the error calculations. It must be noticed that diagnostics are only used here to define the beam position and are not used for beam matching purposes. Some of them will be used in real conditions as beam matching and beam alignment devices. In the case of this report, due to the fact that we have chosen not to re-tune the beam for each error run, the diagnostics listed in Table 2 are used only for beam alignment (position determination).

Name	Type	Length
	DRIFT	779
	DRIFT	431
	DRIFT	300
LR1-Q505	QUAD_ELE	200
	DRIFT	100
LR1-Q506	QUAD_ELE	100
LR1-Q506	QUAD_ELE	100
	DRIFT	100
LR1-Q507	QUAD_ELE	200
	DRIFT	300
LR1-DC53-VE	THIN_STEERING	0
LR1-DC53-HO	THIN_STEERING	0
	DRIFT	431
	DRIFT	779
LR1-PR55	DIAG_POSITION	0
	DRIFT	779
	DRIFT	11
LR1-DC54-VE	THIN_STEERING	0
LR1-DC54-HO	THIN_STEERING	0
	DRIFT	300
LR1-Q508	QUAD_ELE	200
	DRIFT	100
LR1-Q509	QUAD_ELE	100
LR1-Q509	QUAD_ELE	100
	DRIFT	100
LR1-Q510	QUAD_ELE	200
	DRIFT	300
	DRIFT	11
	DRIFT	779
D2	DIAG_POSITION	0
	DRIFT	779
D3	DIAG_POSITION	0
	DRIFT	475.5
	DRIFT	300
LRD-Q11	QUAD_ELE	200
	DRIFT	100
LRD-Q12	QUAD_ELE	100
LRD-Q12	QUAD_ELE	100
	DRIFT	100
LRD-Q13	QUAD_ELE	200
	DRIFT	300
LRD-DC11-VE	THIN_STEERING	0
LRD-DC11-HO	THIN_STEERING	0
	DRIFT	475.5
	DRIFT	779
D4	DIAG_POSITION	0
	DRIFT	779

Continuation 1

	DRIFT	475.5
	DRIFT	300
LRD-Q14	QUAD_ELE	200
	DRIFT	100
LRD-Q15	QUAD_ELE	100
LRD-Q15	QUAD_ELE	100
	DRIFT	100
LRD-Q16	QUAD_ELE	200
	DRIFT	300
LRD-DC12-VE	THIN_STEERING	0
LRD-DC12-HO	THIN_STEERING	0
	DRIFT	475.5
	DRIFT	779
D5	DIAG_POSITION	0
	DRIFT	234.31
LRD-DE21	BEND_ELE	314.16
	DRIFT	300.31
D6	DIAG_POSITION	0
	DRIFT	1100
LRD-Q201	QUAD_ELE	200
	DRIFT	100
LRD-Q202	QUAD_ELE	200
	DRIFT	1350
	DRIFT	1050
	DRIFT	300
LRD-Q203	QUAD_ELE	200
	DRIFT	100
LRD-Q204	QUAD_ELE	200
	DRIFT	1600
D7	DIAG_POSITION	0
	DRIFT	1655
LRD-Q205	QUAD_ELE	200
	DRIFT	100
LRD-Q206	QUAD_ELE	200
	DRIFT	1589
DC-VE_05	THIN_STEERING	0
DC-HO_05	THIN_STEERING	0
	DRIFT	300
LRD-Q207	QUAD_ELE	200
	DRIFT	811
LRD-Q208	QUAD_ELE	100
LRD-Q208	QUAD_ELE	100
	DRIFT	811
LRD-Q209	QUAD_ELE	200
	DRIFT	300
D8	DIAG_POSITION	0

Continuation 2

	DRIFT	1589
LRD-Q210	QUAD_ELE	200
	DRIFT	100
LRD-Q211	QUAD_ELE	200
	DRIFT	1600
DC-VE_06	THIN_STEERING	0
DC-HO_06	THIN_STEERING	0
	DRIFT	1655
LRD-Q212	QUAD_ELE	200
	DRIFT	100
LRD-Q213	QUAD_ELE	200
	DRIFT	300
D9	DIAG_POSITION	0
	DRIFT	1050
	DRIFT	1350
LRD-Q214	QUAD_ELE	200
	DRIFT	100
LRD-Q215	QUAD_ELE	200
	DRIFT	300.31
DC-VE_07	THIN_STEERING	0
DC-HO_07	THIN_STEERING	0
	DRIFT	1100
LRD-DE22	BEND_ELE	314.16
	DRIFT	234.31
D10	DIAG_POSITION	0
	BEAM_ROT	0
	DRIFT	1E-08
	DRIFT	400
LRD-DE31	BEND_ELE	628.32
	DRIFT	500
	DRIFT	250
LRD-Q41	QUAD_ELE	200
	DRIFT	100
LRD-Q42	QUAD_ELE	200
	DRIFT	249
DC-VE_08	THIN_STEERING	0
DC-HO_08	THIN_STEERING	0
	DRIFT	249
LRD-Q43	QUAD_ELE	200
	DRIFT	400
D11	DIAG_POSITION	0
	DRIFT	277
LRD-Q44	QUAD_ELE	100
LRD-Q44	QUAD_ELE	100
	DRIFT	277
	DRIFT	400
LRD-Q45	QUAD_ELE	200

Continuation 3

	DRIFT	249
DC-VE_09	THIN_STEERING	0
DC-HO_09	THIN_STEERING	0
	DRIFT	249
LRD-Q46	QUAD_ELE	200
	DRIFT	100
LRD-Q47	QUAD_ELE	200
	DRIFT	250
D12	DIAG_POSITION	0
	DRIFT	500
LRD-DE41	BEND_ELE	628.32
	DRIFT	400
D13	DIAG_POSITION	0
	DRIFT	1E-08
	BEAM_ROT	0
	DRIFT	779
	DRIFT	242
DC-VE_10	THIN_STEERING	0
DC-HO_10	THIN_STEERING	0
	DRIFT	200
LRD-Q501	QUAD_ELE	200
	DRIFT	100
LRD-Q502	QUAD_ELE	200
	DRIFT	200
	DRIFT	400
	DRIFT	400
DC-VE_11	THIN_STEERING	0
DC-HO_11	THIN_STEERING	0
	DRIFT	200
LRD-Q503	QUAD_ELE	200
	DRIFT	100
LRD-Q504	QUAD_ELE	200
	DRIFT	200
	DRIFT	242
	DRIFT	779
D14	DIAG_POSITION	0
	DRIFT	779
D15	DIAG_POSITION	0
	DRIFT	271
LRD-Q505	QUAD_ELE	200
	DRIFT	100
LRD-Q506	QUAD_ELE	100
LRD-Q506	QUAD_ELE	100
	DRIFT	100
LRD-Q507	QUAD_ELE	200
	DRIFT	271

Continuation 4

DC-VE_12	THIN_STEERING	0
DC-HO_12	THIN_STEERING	0
	DRIFT	779
D16	DIAG_POSITION	0
	DRIFT	779
	DRIFT	271
LRD-Q508	QUAD_ELE	200
	DRIFT	100
LRD-Q509	QUAD_ELE	100
LRD-Q509	QUAD_ELE	100
	DRIFT	100
LRD-Q510	QUAD_ELE	200
	DRIFT	271
DC-VE_13	THIN_STEERING	0
DC-HO_13	THIN_STEERING	0
	DRIFT	779
D17	DIAG_POSITION	0
	DRIFT	779
D18	DIAG_POSITION	0
	DRIFT	541
LRD-Q61	QUAD_ELE	200
	DRIFT	100
LRD-Q62	QUAD_ELE	100
LRD-Q62	QUAD_ELE	100
	DRIFT	100
LRD-Q63	QUAD_ELE	200
	DRIFT	541
DC-VE_14	THIN_STEERING	0
DC-HO_14	THIN_STEERING	0
	DRIFT	779
D19	DIAG_POSITION	0
	DRIFT	779
	DRIFT	541
LRD-Q64	QUAD_ELE	200
	DRIFT	100
LRD-Q65	QUAD_ELE	100
LRD-Q65	QUAD_ELE	100
	DRIFT	100
LRD-Q66	QUAD_ELE	200
	DRIFT	541
DC-VE_15	THIN_STEERING	0
DC-HO_15	THIN_STEERING	0
	DRIFT	779
D20	DIAG_POSITION	0
	BEAM_ROT	0
	DRIFT	1E-08
	DRIFT	400

Continuation 5

LRD-DE61	BEND_ELE	628.32
	DRIFT	200
	DRIFT	247.07
DC-VE_16	THIN_STEERING	0
DC-HO_16	THIN_STEERING	0
	DRIFT	200
LRD-Q71	QUAD_ELE	200
	DRIFT	277.93
LRD-Q72	QUAD_ELE	100
LRD-Q72	QUAD_ELE	100
	DRIFT	277.93
LRD-Q73	QUAD_ELE	200
	DRIFT	200
	DRIFT	247.07
D21	DIAG_POSITION	0
	DRIFT	200
LRD-DE71	BEND_ELE	628.32
	DRIFT	400
D22	DIAG_POSITION	0
	DRIFT	1E-08
	BEAM_ROT	0
	DRIFT	779
	DRIFT	21
DC-VE_17	THIN_STEERING	0
DC-HO_17	THIN_STEERING	0
	DRIFT	200
ARD-Q11	QUAD_ELE	200
	DRIFT	100
ARD-Q12	QUAD_ELE	200
	DRIFT	200
	DRIFT	300
	DRIFT	300
DC-VE_18	THIN_STEERING	0
DC-HO_18	THIN_STEERING	0
	DRIFT	200
ARD-Q13	QUAD_ELE	200
	DRIFT	100
ARD-Q14	QUAD_ELE	200
	DRIFT	221
	DRIFT	779
D23	DIAG_POSITION	0
	DRIFT	779
D24	DIAG_POSITION	0

Table 2 : Detailed beam line structure; in red the quadrupoles, in green the steerers, in blue the position diagnostics.

c Input Beam characteristics

The beam specifications at the entrance of the beam line consider a $^{122}Sn^{1+}$ ion beam at 60keV with $RMS_{X,Y}$=3mm, $RMS_{X',Y'}$=6.67mrad and $\alpha_{X,Y}$=0. The transverse beam emittance is therefore 20mm.mrad (80mm.mrad at 2 RMS). Details of the beam optics are given in Table 3. Particle distributions are taken as Gaussians. The beam energy spread considered is $2.0 * 10^{-4}$ %.

X-X'
Emit [rms] = 0.0206 Pi.mm.mrad [Norm.]
Beta = 0.4472 mm/Pi.mrad
Alpha = -0.0000
Y-Y'
Emit [rms] = 0.0206 Pi.mm.mrad [Norm.]
Beta = 0.4531 mm/Pi.mrad
Alpha = -0.0000

Beam Speed
Beta = 0.001027998 Gamma = 1.000000528
Mo = 113552.36110000 MeV

Beam Matrix (unit : meter, radian)

8.9557307e-06	0	0	0	0	0
0	4.4776498e-05	0	0	0	0
0	0	9.0842616e-06	0	0	0
0	0	0	4.4240545e-05	0	0
0	0	0	0	3.0657834e-06	0
0	0	0	0	0	1.0072209e-12

Table 3: Beam specifications at the entrance of the beam line.

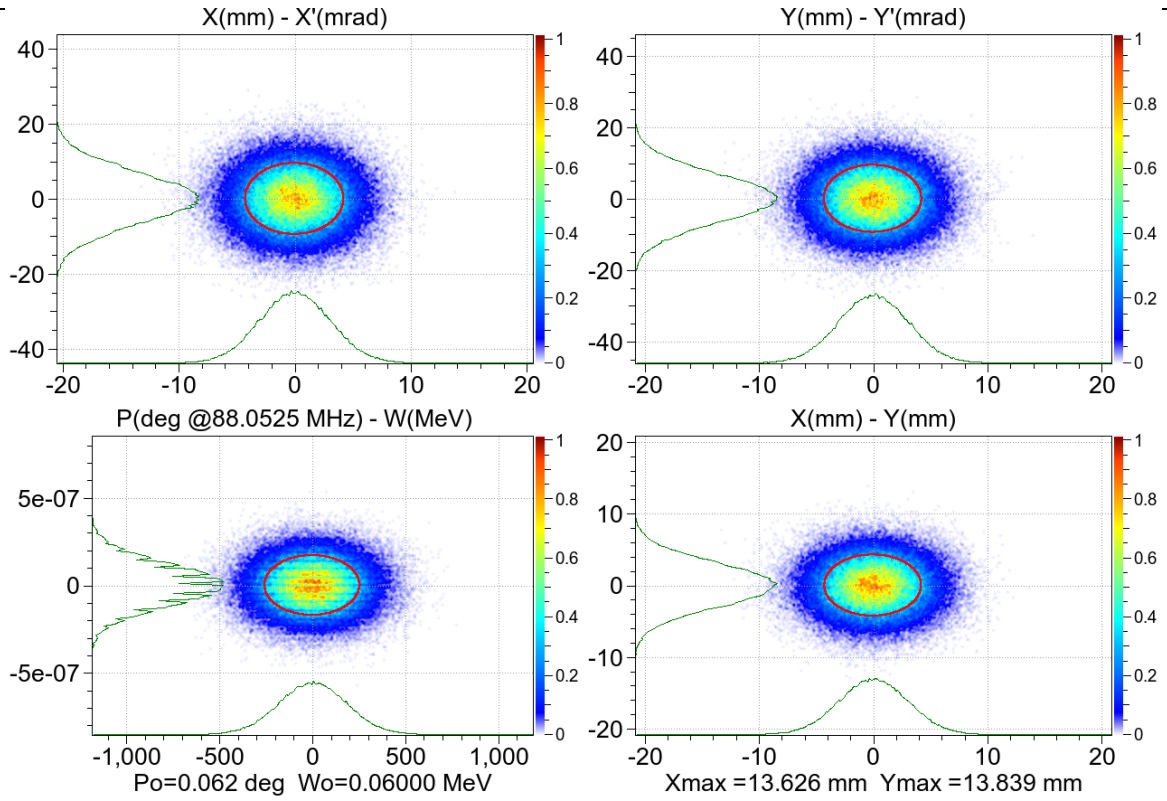

Figure 5: Beam characteristics at the entrance of the beam line for X, Y, X', Y' momentum and energy.

d Nominal Optics

We do not give here the methodology for the beam tuning which has been described in details in [2, 4]. The beam is transported from waist to waist from one sub-section to another (through sextuplet, deviation or re-adaptation sections). Each section is matched independently. Beam alignment is done for each section independently for time consumption reasons and to mimic as well as possible the real beam tuning conditions.

From the given 60 keV beam energy, we can determine its associated momentum P=116.73MeV/c. The radius of deflection is ρ=0.4m. Therefore, we can determine the needed field gradient required to deviate the $^{122}Sn^{1+}$ beam at 60keV:

Table 4 shows the nominal voltages which have to be applied to the quadrupoles for transporting the $^{122}Sn^{1+}$ beam at 60keV.

Quad Name	Voltage between electrodes (V)
LR1-Q505/LR1-Q507/LR1-Q508/LR1-Q510	1962.89
LR1-Q506/LR1-Q509	-3657.81
LRD-Q11/LRD-Q13/LRD-Q14/LRD-Q16	1816.36
LRD-Q12/LRD-Q15	-3412.14
LRD-Q201/LRD-Q215	2896.11
LRD-Q202/LRD-Q214	-2596.51
LRD-Q203/LRD-Q213	1997.32
LRD-Q204/LRD-Q212	-1704.21
LRD-Q205/LRD-Q211	2207.89
LRD-Q206/LRD-Q210	-1997.32
LRD-Q207/LRD-Q209	1428.73
LRD-Q208	-1527.47
LRD-Q41/LRD-Q47	-3395.44
LRD-Q42/LRD-Q46	4397.72
LRD-Q43/LRD-Q45	-3286.69
LRD-Q44	963.082
LRD-Q501	2443.91
LRD-Q502	-2905.41
LRD-Q503	2932.44
LRD-Q504	-2497.91
LRD-Q505/LRD-Q507/LRD-Q508/LRD-Q510	2139.18
LRD-Q506/LRD-Q509	-3950.66
LRD-Q61/LRD-Q63/LRD-Q64/LRD-Q66	1957.25
LRD-Q62/LRD-Q65	-3645.59
LRD-Q71/LRD-Q73	4960.18
LRD-Q72	-5037.31
ARD-Q11	2757.91
ARD-Q12	-3247.44
ARD-Q13	3212.51
ARD-Q14	-2682.25

Table 4: Voltage between electrodes in the quadrupoles.

With these quadrupole settings, the beam envelops and beam line dispersion in the transverse plane are presented on Figures 6 and 7.

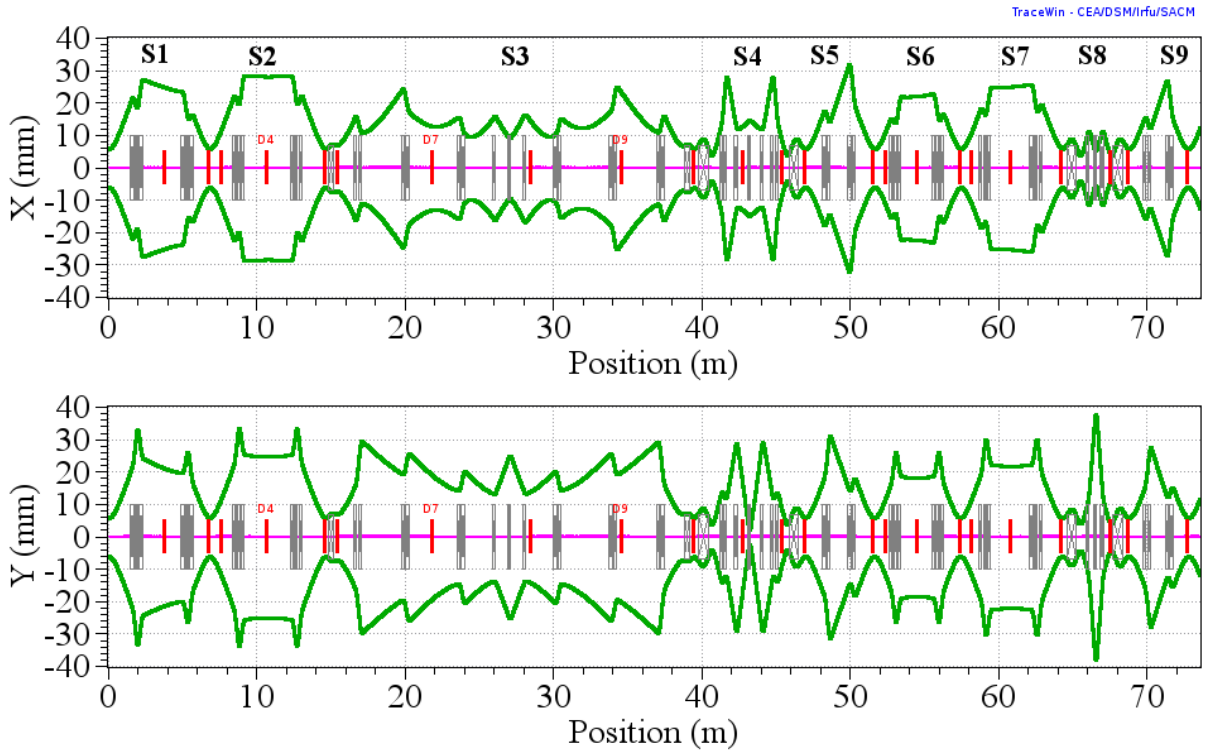

Figure 6: RMS beam envelops in X and Y along the line for the $^{122}Sn^{1+}$ beam with an emittance of 20mm.mrad at one RMS.

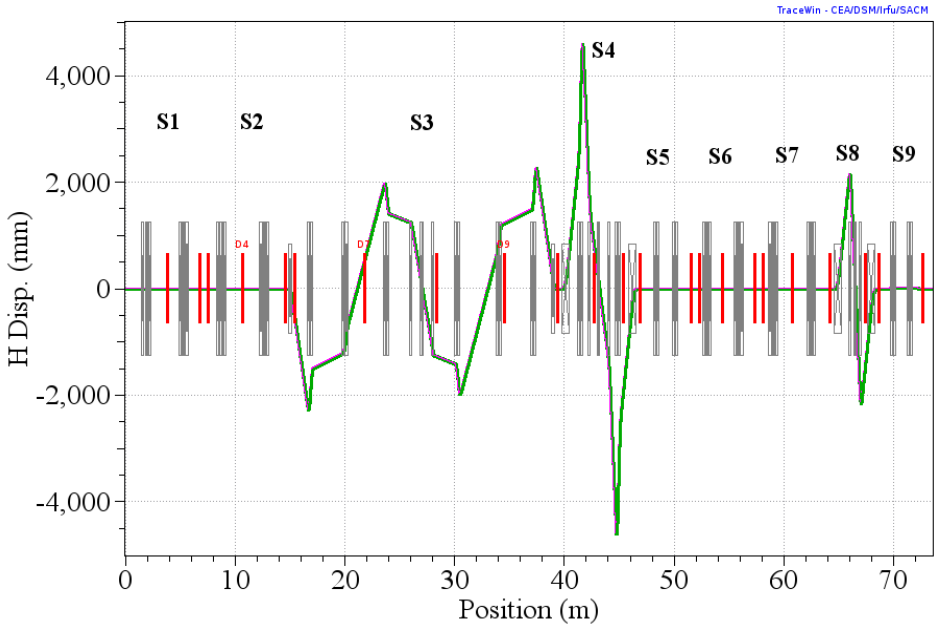

Figure 7: Horizontal RMS beam dispersion along the line.

We can notice that vertical dispersion terms are observed in the horizontal plane and we can observe the same thing in the section transfer matrices (see Table 5). The two vertical deviations (S4 and S8

sections) are technically treated as horizontal deviations: at the entrance of these deviations, the beam is transversally rotated by 90°.

S1

-1.000004	-0.000066	0	0	0	0
0.000018	-0.999996	0	0	0	0
0	0	-1.000014	-0.000171	0	0
0	0	0.000065	-0.999986	0	0
0	0	0	0	1	6.799993
0	0	0	0	0	1

S6

-0.999946	0.017347	0	0	0	0
-0.006274	-0.999946	0	0	0	0
0	0	-0.999997	0.003422	0	0
0	0	-0.001857	-0.999997	0	0
0	0	0	0	1	5.799994
0	0	0	0	0	1

S2

-1.000000	-0.000077	0	0	0	0
0.000017	-1.000000	0	0	0	0
0	0	-1.000000	-0.000144	0	0
0	0	0.000041	-1.000000	0	0
0	0	0	0	1	7.817992
0	0	0	0	0	1

S7

-0.999884	-0.028676	0	0	0	0
0.008084	-0.999884	0	0	0	0
0	0	-0.999994	-0.005662	0	0
0	0	0.002133	-0.999994	0	0
0	0	0	0	1	6.879993
0	0	0	0	0	1

S3

0.156045	0.462522	0	0	0	-0.0001545
-2.109412	0.156045	0	0	0	0.000281914
0	0	-0.996446	0.040051	0	0
0	0	-0.177135	-0.996446	0	0
0.000281914	-0.0001545	0	0	1	24.682644
0	0	0	0	0	1

S8

-0.515528	0.385880	0	0	0	-0.00339467
-1.902744	-0.515528	0	0	0	0.013332428
0	0	0.615347	0.363718	0	0
0	0	-1.708325	0.615347	0	0
0.013332428	-0.00339467	0	0	1	3.565238
0	0	0	0	0	1

S4

-0.523135	0.381548	0	0	0	0.000112377
-1.903638	-0.523135	0	0	0	-0.00044861
0	0	-0.280659	-0.446281	0	0
0	0	2.064241	-0.280659	0	0
-0.00044861	0.000112377	0	0	1	6.594299
0	0	0	0	0	1

S9

-0.994454	0.115378	0	0	0	0
-0.649724	-0.930195	0	0	0	0
0	0	-0.943669	0.141298	0	0
0	0	-0.668317	-0.959624	0	0
0	0	0	0	1	3.999996
0	0	0	0	0	1

S5

-0.938917	0.145942	0	0	0	0
-0.590799	-0.973224	0	0	0	0
0	0	-0.961583	0.121537	0	0
0	0	-0.578934	-0.966779	0	0
0	0	0	0	1	4.641995
0	0	0	0	0	1

Full Matrix Transfer

0.394135	-0.450163	0	0	0	0.004767038
1.933320	0.329051	0	0	0	-0.01085384
0	0	0.036723	0.461611	0	0
0	0	-2.163067	0.040965	0	0
0.013494085	-0.0033174	0	0	1	70.782139
0	0	0	0	0	1

Table 5: Transfer matrix of the whole beam line. Units: meter, rad, dp/p.

II Error studies

a Introduction

Error studies are important in order to evaluate the contributions to spreads and deviations of the beam optics originating from:

- the input beam characteristics: shifts (positions, energy), emittance growth, beam mismatches
- the quadrupoles settings: position, rotation around axis, field gradient
- the precision on diagnostics measurements: position, size

Impact on beam tuning, losses and optical characteristics along the lines must be evaluated. With the TraceWin code, two types of errors can be computed: static and dynamic errors. Static errors are detectable and can be corrected for. For instance, the determination of the beam position with harps monitors can be used to compensate by means of steerers the beam misalignments induced by quadrupoles. Dynamic errors (noises, vibrations) are not corrected for in the present study, since their amplitudes are typically lower by a factor 10.

In this report, we study the contributions of the input beam characteristics as a first step, taking into account the accuracy of beam diagnostics (beam position precision). The corresponding tolerances are

summarized in Tables 6 and 7. The TraceWin code was run using beam input values randomly and uniformly distributed between ±1 times the maximum values taking into account the tolerances.

Error type	Static
Displacement dx, dy (mm)	±0.25
Displacement dx', dy' (mrad)	±0.25
Longitudinal displacement dφ (°), dE (eV)	±0.002°, ±6eV
Transverse emittance growth (%)	±1
Longitudinal emittance growth (%)	±0.1
Transverse mismatch (%)	±1
Longitudinal mismatch (%)	±0.1
Current (nA)	±1

Table 6: Error amplitudes associated to the input beam characteristics. "Displacement" means that the beam position is not centered. "Emittance growth" means that the input beam emittance is increased by a given percentage. Transverse or longitudinal "Mismatch" means that the beam input is mismatched by a given percentage: we have chosen here 1%; therefore beam twiss parameters α_x and β_x (see Table 3) are multiplied by 100.

Error type	Value
Position precision (mm)	±0.5

Table 7: Tolerance on the position determination.

We present in the following the results obtained for 2000 runs for a $^{122}Sn^{1+}$ beam at 60keV and characterized by the previously introduced types and amplitudes of error. For the beam position correction, we use in the beam line 15 pairs of horizontal and vertical electrostatic steerers (simultaneous bi-dimensional correction at each location). Beam size optimizations are performed with the 23 two-dimensional beam profilers.

Useful results are beams characteristics fluctuations along the line. It is also interesting to have an estimate of the working range of the different correctors used to realign the beam.

b Beam alignment corrections

This calculation provides the beam alignment corrections to be applied using steerers in order to deal with the input beam errors. Quadrupoles fields are not readapted at each run in order to respect the criteria (sizes and waist) given in section Id. Errors on quadrupole settings are not taken into account.

Figure 8 shows the transverse average and RMS beam orbit over the 2000 calculations. We can remark that the fluctuation of the average is less than 0.1mm and the RMS to the beam center fluctuation over the 2000 calculation is less than 0.5mm. The fluctuation of the residual orbit is small all along the line. We can remark that the position distribution of the beam center is larger for the beam line part up to Z=50m, whereas beyond this position in Z the distribution becomes smaller.

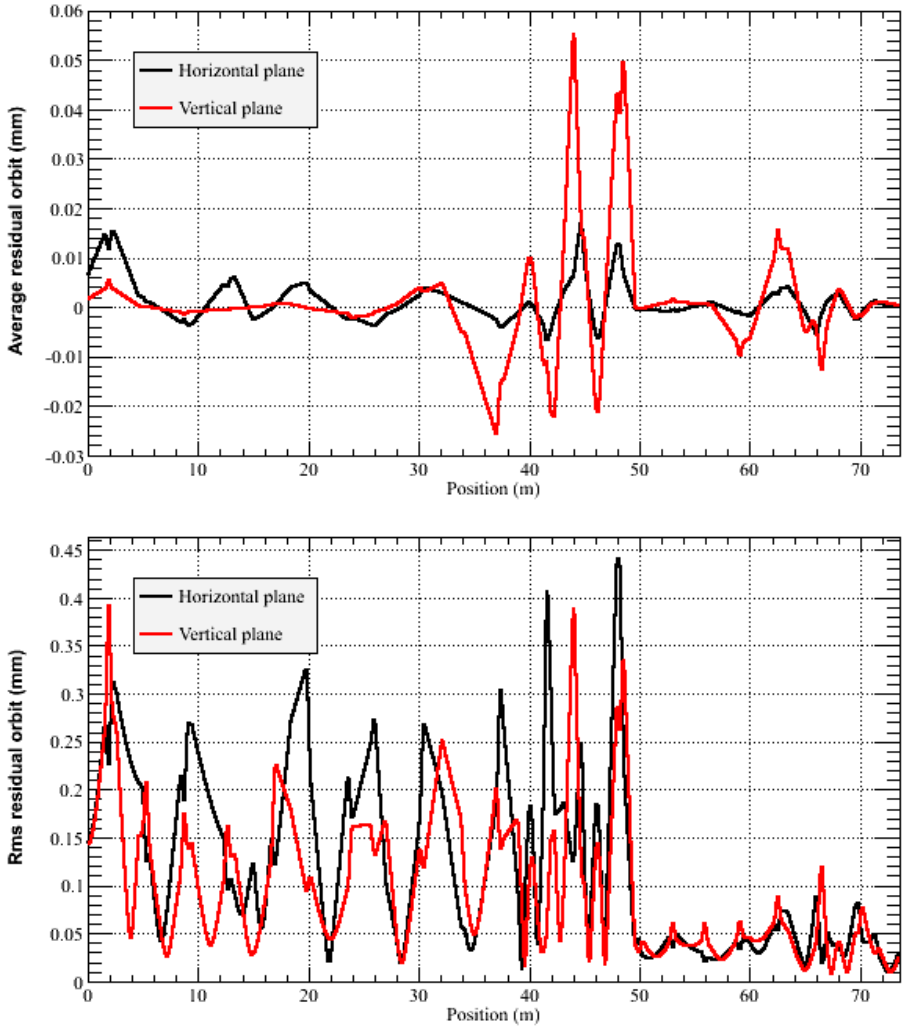

Figure 8: Transverse average and RMS beam orbits along the line.

In Figure 9 and Table 6, we present the steerers settings for the beam re-alignment. The mean values of the steerers in the first vertical section S4 (DC-VE_08, DC-HO_08, DC-VE_09, DC-HO_09) and in the first re-adaptation section S5 (DC-VE_10, DC-HO_10, DC-VE_11, DC-HO_11) are systematically higher than 1V in absolute value especially for the horizontal correctors. Therefore, the RMS values of the steerer corrections are relatively large from 10V up to 50V. But RMS steerer voltages in the next sections of the beam line are less than 10V.

These results tell us that:

- an original input beam misalignment can be reasonably well compansated using dedicated steerers
- the left-right 45° beam line (S4) amplifies significantly any original misalignment, which means that the steerers location in the S4 section may not be very well optimized
- the contribution of the steerers located in the first re-adaptation section (S5) is very important and their location is presumably already optimized.

STEERER Name	Mean (V)	RMS (V)
LR1-DC53-VE	-0.24	10.85
LR1-DC53-HO	-0.05	21.24
LR1-DC54-VE	0.65	9.21
LR1-DC54-HO	0.14	22.95
LRD-DC11-VE	0.29	6.38
LRD-DC11-HO	-0.01	11.87
LRD-DC12-VE	-0.63	6.00
LRD-DC12-HO	-0.04	12.41
DC-VE_04	-0.22	9.64
DC-HO_04	-0.05	3.64
DC-VE_05	-0.05	4.31
DC-HO_05	0.16	10.77
DC-VE_06	-0.07	4.90
DC-HO_06	-0.82	16.07
DC-VE_07	0.00	2.09
DC-HO_07	0.63	3.22
DC-VE_08	0.31	9.26
DC-HO_08	3.06	31.45
DC-VE_09	-0.51	9.73
DC-HO_09	1.51	13.88
DC-VE_10	-1.53	47.59
DC-HO_10	-7.08	46.21
DC-VE_11	0.70	23.81
DC-HO_11	5.83	35.47
DC-VE_12	0.02	0.25
DC-HO_12	0.01	0.25
DC-VE_13	-0.13	1.35
DC-HO_13	-0.31	1.29
DC-VE_14	0.26	3.24
DC-HO_14	0.72	2.38
DC-VE_15	-0.39	4.84
DC-HO_15	-1.44	3.18
DC-VE_16	-0.60	5.99
DC-HO_16	-1.18	1.54
DC-VE_17	0.49	7.79
DC-HO_17	0.80	9.87
DC-VE_18	-0.19	4.34
DC-HO_18	-0.36	5.63

Table 6 : Mean and RMS values of the eletrical fields (V) of the steerers.

Figures 10 and 11 and Table 7 show that the beam stability at the end of the line is relatively well preserved once the steerer corrections are applied. As a consequence, the transverse positions are maintained, the beam remaining centered in X and Y ($<\pm 0.1$mm, $<\pm 0.1$mrad).

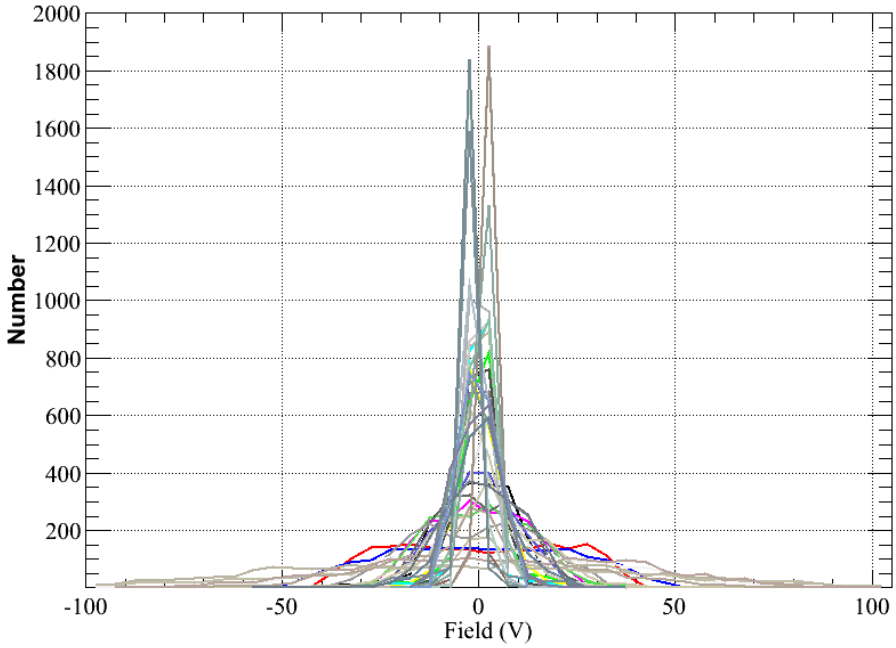

Figure 9: Steerer electric fields distributions for the 2000 calculations.

Nevertheless the beam size is around 6mm in horizontal and vertical which is two times larger than the RMS beam size at the beginning of the line. This larger size is, however, known with a good precision (less than 0.04mm). This increase of the beam size is not yet well understood, the beam divergence remaining close to the nominal one, defined at the beginning of the line (see section Ic).

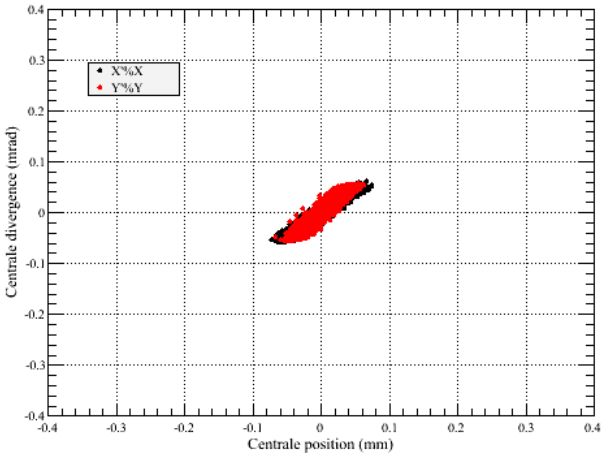

Figure 10: X and Y central position and divergence of the beam at the end of the beam line for the 2000 calculations.

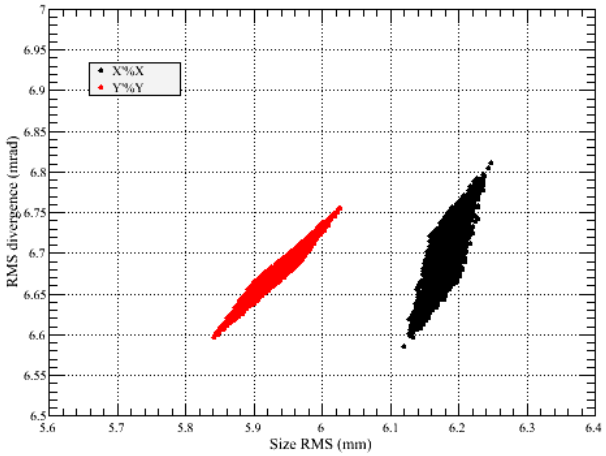

Figure 11: X and Y RMS size and divergence of the beam at the end of the beam line for the 2000 calculations.

Type	Mean Position	RMS Position	Mean Size	RMS Size
X (mm)	**0.0**	**0.03**	**6.18**	**0.02**
Y (mm)	**0.0**	**0.03**	**5.93**	**0.04**
X' (mrad)	0.0	0.03	6.7	0.04
Y' (mrad)	0.0	0.03	6.67	0.03

Table 7: Mean and RMS of the beam position at the end of the line.

Conclusions

In this calculation, we have summarized the error calculations done along the 73m transfer beam line from the adaptation point in the SPIRAL2 production building up to the adaptation point in the DESIR building. We have treated, arbitrarily, the case of a $^{122}Sn^{1+}$ beam at 60keV with a typical geometric transverse emittance of 20 π mm.mrad.

The error calculations have beam performed taking into account input beam misalignments (position, emittance growth, energy spread …). We did not present the calculation results including quadrupoles errors and beam matching corrections performed by retuning the quadrupoles. The present calculation was indeed focused on the possibility to overcome original misalignments and to realign the beam using steerers only.

We have remarked that the RMS fields on steerers need to be increased along the line in order to ensure the beam stability. The first vertical deviation (6.25m high) and the first re-adaptation section are crucial in the beam alignment procedure. The amplitudes of the steerer fields are relatively large (up to 50V RMS).

With these types of errors and without quadrupole matching, the beam size at the end of the line (i.e. in the DESIR building) is two times larger than the input beam transverse size. This result is not yet completely understood.

A steerer implementation optimization in the horizontal left-right and the first vertical deviations must be done and its effect on the beam alignment must be checked in order to reduce as much as possible the steerer field amplitudes.

Error calculations must be conducted taking into account as well the quadrupole errors in order to test the possibility to realign the beam when all errors are combined.

References

[1] TraceWin code: http://irfu.cea.fr/Sacm/logiciels/index.php

[2] F. Varenne, Architecture optique des lignes de transport faisceaux 1+ vers le hall DESIR, EDMS I-020986_v2.0

[3] Références dimensionnelles du procédé Transport Faisceau de SPIRAL2 rapporté au référentiel géodésique du GANIL, EDMS I-017095_v2.0

[4] L. Perrot, Références optiques des lignes de transport des faisceaux 1+ vers le hall DESIR. Transcription pour le code TRANSPORT : EDMS I-025427

APPENDIX 3

MLLtrap test and progress report

Improving the performance of the MLLTRAP Penning trap facility

P.G. Thirolf, C. Weber, E. Gartzke, K. Krug, P. Müller, J. Moazzami-Fallah
LMU München, Germany
W. Plass, T. Dickel, C. Jesch
Univ. Giessen, Germany

MLLTRAP mass resolution

The Penning trap mass spectrometer MLLTRAP at the Maier-Leibnitz-Laboratory Garching enables precise mass determination of stable and unstable nuclei with a mass accuracy of $\delta m/m \approx 10^{-8}$ [1]. Commissioning measurements of MLLTRAP with ^{85,87}Rb ions (see Fig. 1) resulted in a measured mass of m(^{85}Rb) = 84.9117959(24) u, corresponding to a relative mass uncertainty of $\delta m/m = 2.9 \cdot 10^{-8}$. The literature value of the mass of ^{85}Rb is 84.911798732(14) u (as measured by the MIT group). The results deviate by about 1.2σ. However, in this result only the statistical error has been included and further studies were conducted to quantify various sources of systematic uncertainties.

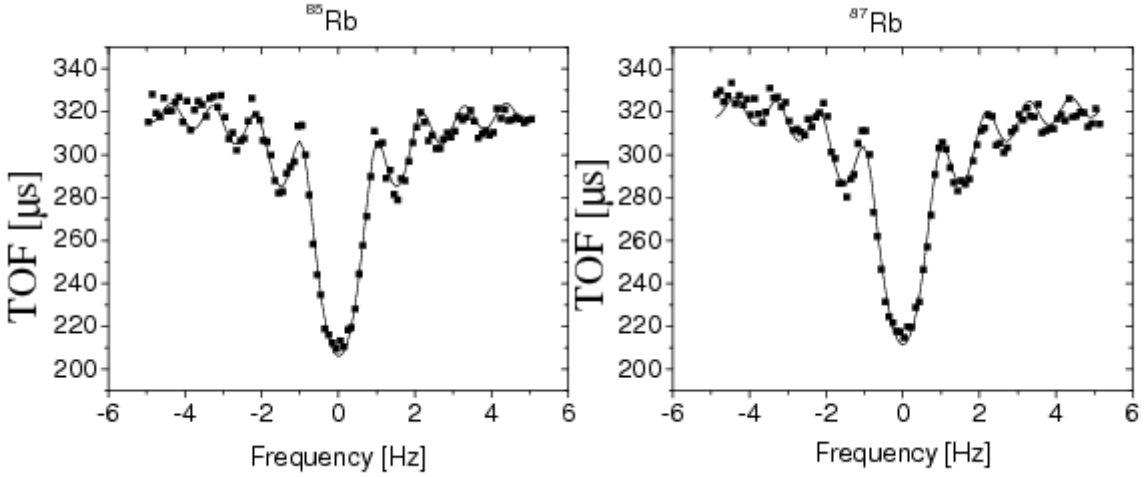

Fig. 1: TOF-ICR resonance curves from mass measurements with MLLTRAP for ^{85}Rb and ^{87}Rb, respectively, with a relative accuracy of 2.9. 10^{-8} prior to the determination of systematic uncertainties [1].

Implementation of an electrostatic quadrupole deflector

An electrostatic quadrupole beam deflector (“4-way beam bender”) has been developed and installed, that allows injecting ions from up to three independent sources [2]. In this way, different offline ion sources as well as a potential extension by a charge breeder device could be accommodated. Using different ion sources is required, e.g., for the production of reference ions for calibrating the magnetic field strength. Fig. 2 shows a trajectory simulation (SIMION) for ^{85}Rb ions starting from the ion source and being transmitted under 90^{o} through the bender and adjacent ion-optical elements.

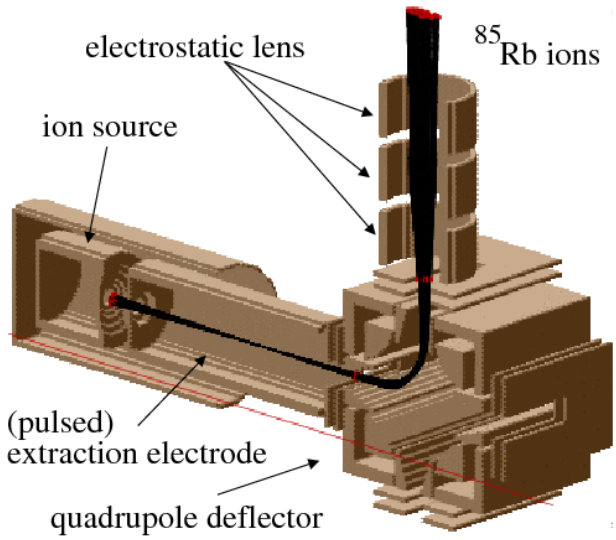

Fig. 2: Trajectory simulation for ^{85}Rb ions transmitted from the ion source across the 90 degree electrostatic quadrupole deflector and a focusing Einzel lens.

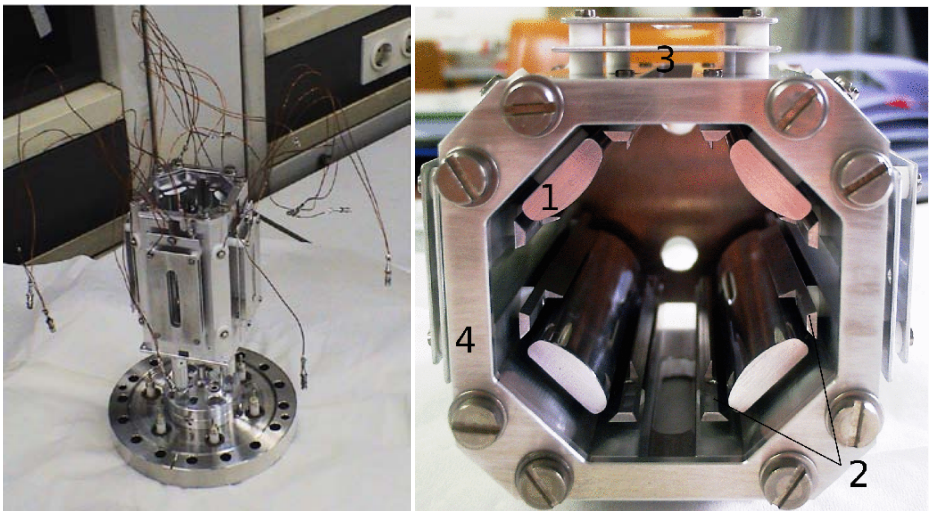

Fig. 3: Photographs of the electrostatic quadrupole deflector.

The transmission efficiency of the deflector was determined to be 75% of the non-deflected ion beam for $^{85}Rb^{+}$ ions [2].

Characterization of magnetic field variations

Variations of the magnetic field of the superconducting 7 T magnet have been studied using ^{85}Rb ions as part of a characterization of the systematic uncertainty of the MLLTRAP system. The long-term fluctuations due to the 'flux-creep' effect were measured to be $\delta B/\delta t \cdot 1/B = -1.3 \cdot 10^{-9}/h$ (see Fig. 4).

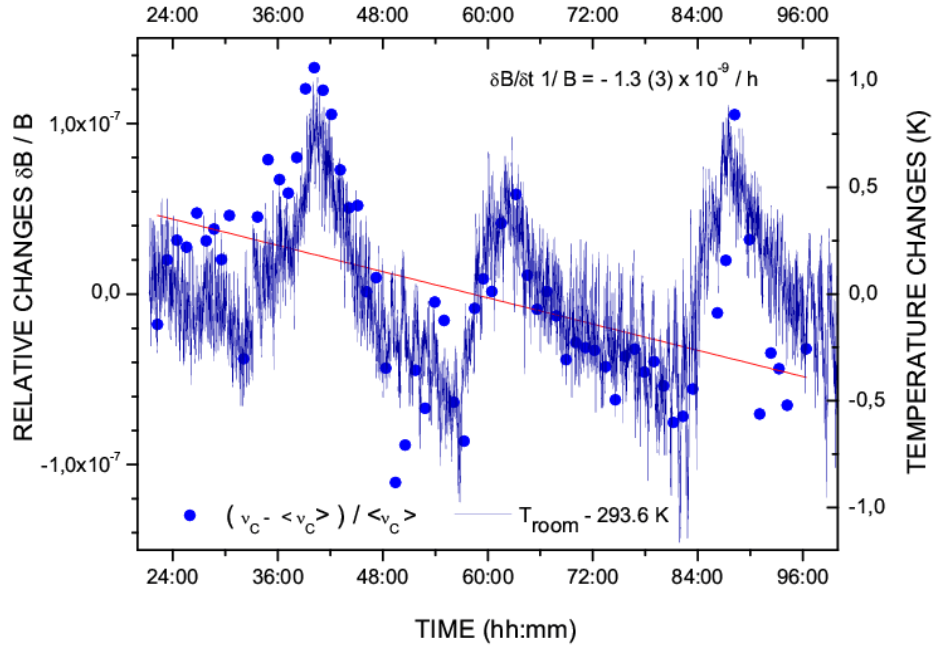

Fig. 4: Correlation between ambient thermal fluctuations and variations of the magnetic field of the Penning trap. The red line indicates the underlying linear decay of the magnetic field according to the 'flux-creep" effect.

The systematic uncertainty contribution of the magnetic field shift was determined to be $\sigma_B(\nu_{ref})/\nu_{ref} = 7.36(38) \cdot 10^{-9}$/h. Finally, this results in a mass value for ^{85}Rb of m(^{85}Rb) = 84.9117959(26) u, indicating that the contribution of magnetic field fluctuations to the systematic error is small. Moreover, the remaining difference of 1.1σ between measured and published mass indicates that systematic errors at MLLTRAP are reasonably well under control [2].

Implementation of Temperature- and Pressure Stabilization at MLLTRAP

Fluctuations of the magnetic field are induced by temperature and pressure variations and represent the main limitations in high-accuracy Penning-trap based mass measurements. For this reason, systems for the stabilization of the temperature in the warm bore and the pressure in the helium reservoir of the MLLTRAP magnet were developed and installed [3]. The working principle of the stabilization systems is a feedback control loop based on a PID (proportional integral derivative) algorithm, which is integrated in the employed controllers. The temperature is stabilized by ventilating the warm bore of the magnet with ambient air, which is heated by a PID-controlled heating element consisting of ceramic resistors. The feedback reading for the control loop is provided by a resistive thermometer situated in the magnet's bore. The pressure in the helium reservoir of the magnet's cryostat is stabilized by exhaust control of the evaporating helium in the reservoir via an electrically driven control valve connected to the helium exhaust, which is actuated according to the pressure reading of a capacitive pressure sensor. The temperature and pressure, as well as the respective control signals were monitored and recorded via a LabVIEW-based control program. Special security measures in order to protect the sensitive 7-T superconducting magnet were applied. Overheating inside the magnet's bore is excluded by integrating temperature delimiters, which disconnect the heating circuit via electromagnetic relays once the temperature exceeds a certain limit. A poppet valve connected as a bypass to the control valve prevents an uncontrolled pressure

increase in the helium reservoir. The adjustable parameters of the control loops were manually tuned for improved response of the stabilization systems. A stabilization of the temperature and pressure within standard deviations of $\Delta T = \pm 2$ mK and $\Delta p = \pm 0.08$ hPa was achieved. The respective peak-to-peak variations were $\Delta T = \pm 6$ mK and $\Delta p = \pm 0.2$ hPa, respectively. In long-term stabilization tests, the bore temperature stability was found to be sensitive to the ambient hall temperature changes, with peak-to-peak variations of about ±10 mK and up to ±25 mK during strong increase of the ambient hall temperature [3]. The obtained precision of the installed stabilization systems at MLLTRAP is comparable to those reported for the regulation systems at other Penning trap facilities. Previous studies of systematic uncertainties at MLLTRAP allow for an estimate of the expected improved magnetic field stability due to the implemented temperature stabilization of down to at least $\Delta B/B = 7 \cdot 10^{-9}$, when considering the highest observed peak-to-peak variations during temperature stabilization. With a combined temperature and pressure stabilization, the standard deviation of the magnetic field fluctuations at MLLTRAP can be expected to be reduced by two orders of magnitude to about $\sigma_B(\nu_{ref})/\nu_{ref} = 2 \cdot 10^{-11}$/h, based on the reduction factor found at the SHIPTRAP facility [4]. Hence, due to the implemented stabilization measures, the contribution of the systematic magnetic field uncertainty to the overall accuracy limit can be expected to be smaller than the envisaged mass accuracy in the range of 10^{-9}.

Development of a beam diagnostic unit and a quadrupole mass analyzer

Optimizing the injection condition into the trap or any other subsequent component like a charge breeder or a multi-reflection time-of-flight mass spectrometer (MRTOF, [5])
for isobaric purification outside the trap system, a diagnostics of the ions extracted from the gas cell is mandatory. Moreover, it is also desirable to add mass selectivity to the injection beam line prior to the ion transfer e.g. to the MRTOF and the Penning traps.
Therefore a quadrupole mass separator (QMS) together with an in-line diagnostics unit was designed in collaboration with the Giessen group of W. Plaß and set up behind the extraction radiofrequency quadrupole (RFQ) of the buffer gas cell.
Fig. 5 (left and middle part) displays the new in-line diagnostic unit mounted behind the extraction-RFQ. The diagnostics unit consists of a three-fold segmented RFQ ion guide housed inside a DN150CF standard double cross. While the upstream and downstream segments of the RFQ (rod length 127 mm, diameter 11 mm) are fixed inside the vacuum cross, the middle section(rod length 52 mm, diameter 11 mm) has been designed as a moveable part operated via a linear actuator (vertical dynamic range 150 mm, see middle part of Fig. 5). By sliding the middle section up or down, either ion transport can be enabled through the RFQ ion guide or a detector can be put into the beam position allowing for ion diagnostics. Fig. 5 gives an overview of the interior of the diagnostics unit, showing in its left part the fixed-end section of the RFQ together with the guiding frame for the retractable middle section (shown in the central panel of Fig. 5). A novel technique was used for the realization of the RFQ ion guide: instead of segmented stainless steel rods a resistive RFQ was built from polyether-ether-ketone (KETRON PEEK, Angst & Pfister) with a 10% carbon admixture in order to generate electrical conductivity in the otherwise insulating material. Fig.5 (left) shows the resistive RFQ ion guide prior to its mounting into the vacuum cross. This way a potential gradient along the length of the RFQ rods of about 1 % can be generated, counted from the difference between the positive and negative high voltages applied at the ends of the rods via 100 kΩ resistors in parallel for each RF phase. All electrical contacts are provided by Kapton-insulated copper wires. The sliding central element of the diagnostics unit consists of an

aluminum frame carrying the retractable middle part of the RFQ ion guide and a silicon detector for the diagnostics of the ion beam (via α-decay spectroscopy). Alternatively, the Si detector can be replaced by a multichannel plate detector (MCP). The moveable Al frame is sliding in grooves engraved in two opposite guiding blocks made of PEEK. The connection to the linear actuator is kept flexible in order to prevent it from getting stuck in case of slight misalignments.The exact vertical alignment of the sliding segment on the central beam axis can be monitored by 1 mm holes at the beam height position under 90 degrees to the beam axis, traversing the fixed guiding side blocks as well as the sliding aluminum part. Via two opposite viewports light applied at one side can only be seen at the opposite side when the sliding parts is exactly centered on the beam axis. The sliding segment of the diagnostics unit can be seen in the central panel of Fig.5, where in the lower position the ends of the middle segment of the resistive RFQ is visible, while above the back side of the Si ion detector can be seen. In order to collect the α decaying ions (arriving with only few eV kinetic energies) near the detector surface, a thin (1.5 μm) aluminized Mylar foil set to an attractive potential of about 400-500 V is placed in front of the detector surface. In the reaction scenario described above, the RFQ ion guide was operated at a frequency of 895 kHz and an amplitude of 300 V_{pp}, using a second customized RF amplifier as described before. An ambient pressure of 10^{-2} mbar (Helium 5.0) was maintained via a mass flow control of the gas inlet using a mass flow controller (Pfeiffer RVC 300) in combination with a regulated valve (Pfeiffer EVR 116). Pumping of the diagnostics unit is provided by a 400 l/s magnetic turbomolecular pump (Pfeiffer TMU400M).

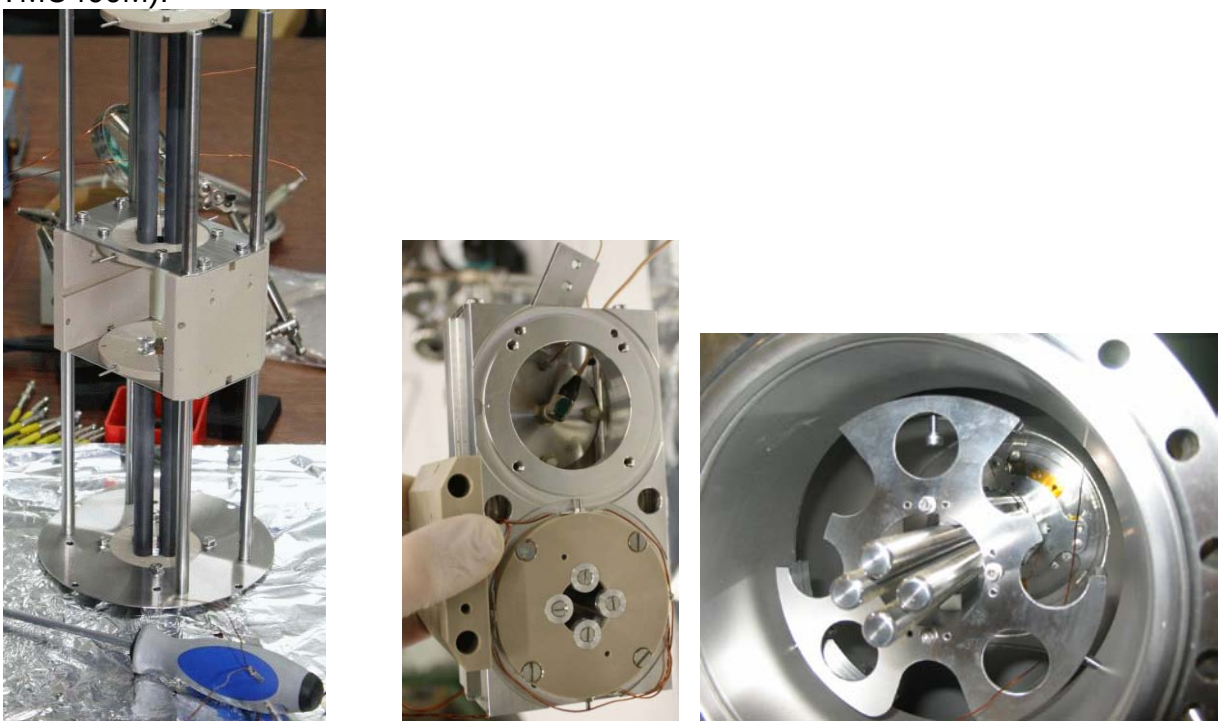

Fig. 5: Photographs of the partitioned RFQ in the diagnostics unit (left) and its sliding middle section with alternative positions for a Si detector and a Faraday cup (central). Right: view to the quadrupole mass separator designed to guarantee mass-selective injection into the Penning trap.

Fig. 6 (left) shows a photograph of the two new components on their support stand.
The QMS (Fig. 5, right) consists of an unsegmented 4-rod radiofrequency quadrupole (rod length 329 mm, diameter 11 mm, inner open diameter 10 mm), housed inside a DN150CF standard cross. Since the extraction RFQ of the buffer gas cell acts as phase spacce cooler using an ambient Helium pressure of about $5 \cdot 10^{-3}$ mbar, while operation of the

subsequent new QMS requires high vacuum better than 10^{-5} mbar, both components are separated by an aperture plate with a narrow opening of 2.5 mm. In addition, the QMS part is pumped by a 1600 l/s turbomolecular pump (Pfeiffer TMU 1601), thus achieving ~10^{-7} mbar in the QMS during ion extraction from the gas cell. Typical operation conditions of the QMS for masses in the range of A~150 (corresponding to the online tests performed via the reaction (^{121}Sb(^{35}Cl,4n)^{152}Er) amount to a frequency of 1215 kHz and an amplitude of 300 V_{pp}. An offset potential of typical a few volts can be applied to adjust the QMS to the exit potential of the extraction RFQ. Since both the QMS and the subsequent diagnostics unit require a linear RF power amplifier, a cost effective, yet powerful solution was realized by modifying a commercial power amplifier designed for use in the amateur radio community. Fig.6 (right) shows a photograph of the amplifier that was realized as a standard rack-mount unit.

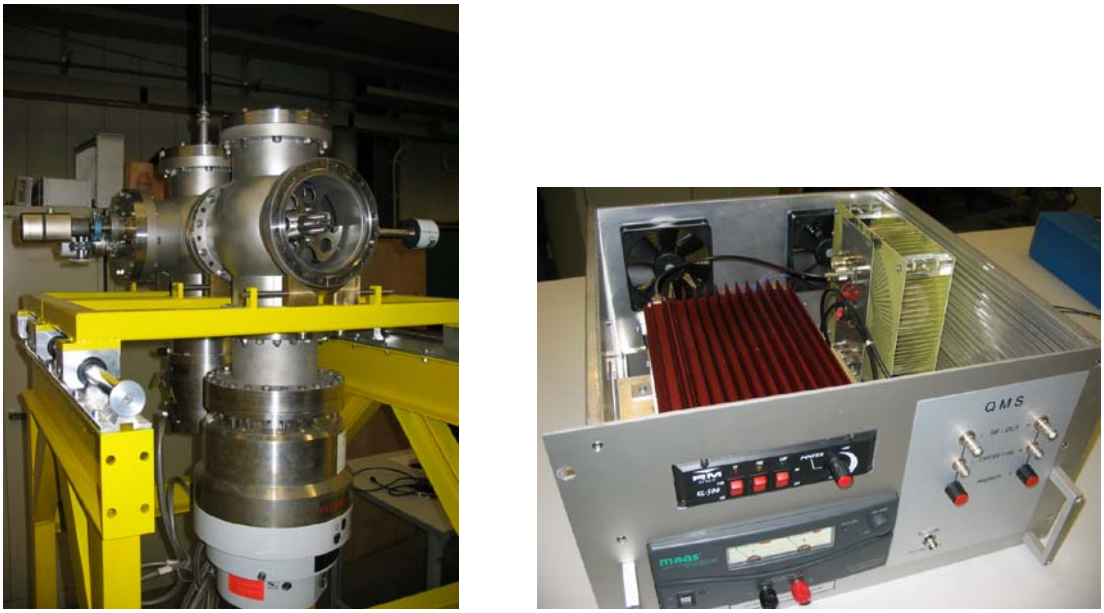

Fig. 6: Left: QMS and diagnostics unit, right: customized RF amplifier designed to provide RF amplitudes up to ~1800 V_{pp}.

Test of a Multi-ReflectionToF spectrometer (MRTOF) at MLLTRAP

When ultimately aiming at using highly-charged ions in the Penning trap, isobaric purification cannot be performed any longer via buffer gas cooling in the first (purification) trap, but instead provisions outside the trap system have to be foreseen. An attractive option is the Multi-Reflection Time-of-Flight Mass Spectrometer (MRTOF) developed by the Giessen group (W. Plass et al. [6]). Fig. 7 shows the principle of the MR-TOF device. Ions transmitted from a radiofrequency quadrupole (RFQ), e.g. a gas-filled stopping cell or the before described QMS, are guided into the system via a curved RFQ. They are cooled and bunched into ion packets in a linear RF trap (injection trap) and injected through a differential pumping stage into the time-of-flight analyzer. They travel in the analyzer for a selectable number of turns, until they are ejected, reflected in a planar ion mirror and fly through a pulsed ion gate for high-resolution separation. After separation, the energy width of the ion beam is reduced in an energy buncher, such that the ions can be injected efficiently into an accumulation trap, which serves to uncouple the repetition rate of the MR-TOF-MS separator from the repetition rate of experiments downstream of

the device. For mass measurements, a microchannel plate (MCP) detector is moved into the ion path instead of the ion gate. Depending on whether the ions are stored in the analyzer for several turns or only pass through the analyzer once, the system can be used for high-resolution mass measurements with limited mass range ($m/\Delta m \geq 10^5$), relative mass range ~2%, or as broadband mass spectrometer ($m/\Delta m \geq 10^3$).

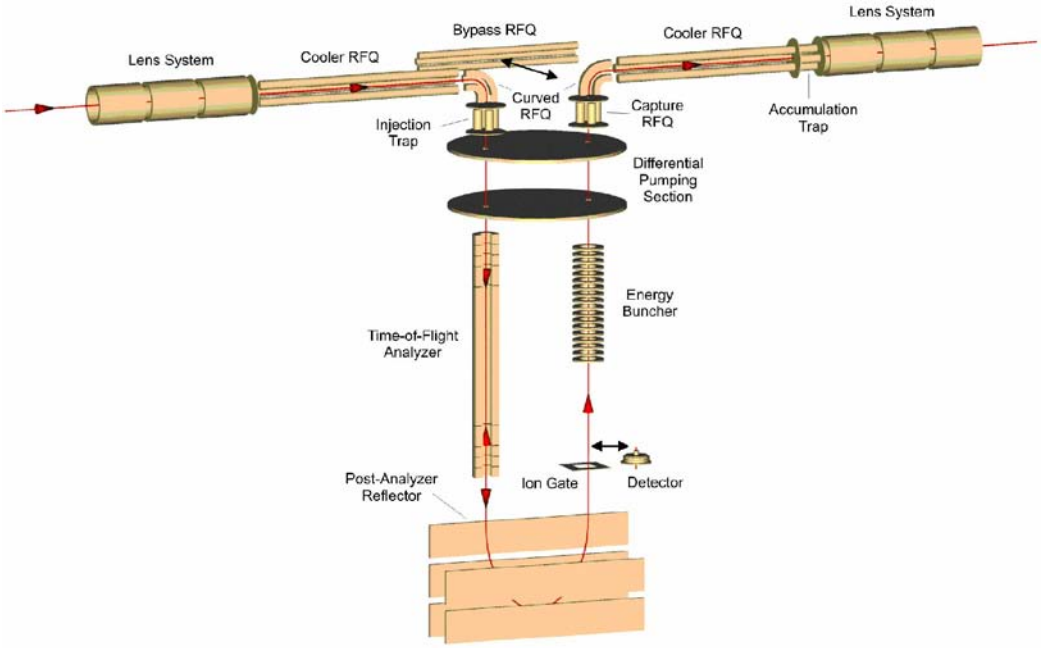

Fig. 7: Schematics of the Multi-Reflection ToF-spectrometer developed by the Giessen group and operated at the Garching Tandem accelerator during a test beamtime.

Tests of an MR-TOF prototype developed by the Giessen group were performed at the Garching Tandem accelerator. The prototype spectrometer was transferred to Garching and coupled to the MLL IonCatcher buffer gas cell [5]. Fig. 8 displays the complete setup installed at the Garching Tandem accelerator. The left picture shows the whole setup with a first 90^o dipole magnet guiding the beam to the target section, followed by a second 90^o dipole used as separation stage between the fusion reaction products and non-reacting primary beam. A quadrupole doublet was used to focus the reaction products into the acceptance of the dipole magnet. Another quadrupole singulet served as focussing element behind the second dipole in front of the entrance window of the buffer gas cell, where the reaction products were thermalized in 50 mbar ultra-pure He gas and, guided by electrical DC and RF fields, extracted through a nozzle orifice into an extraction-RFQ acting as beam cooler followed by the newly constructed QMS and diagnostics unit in front of the MR-TOF device. Finally the right-hand side of Fig.8 shows the MR-TOF prototype coupled to the gas cell at the end of the beamline.

A high mass resolving power of about $m/\delta m \sim 200000$ could be determined for the MRTOF device, clearly qualifying the MRTOF concept not only as applicable for isobaric purification outside the Penning trap system, but also for mass measurements of short-lived nuclear species due to the short measurement times of only a few ms.

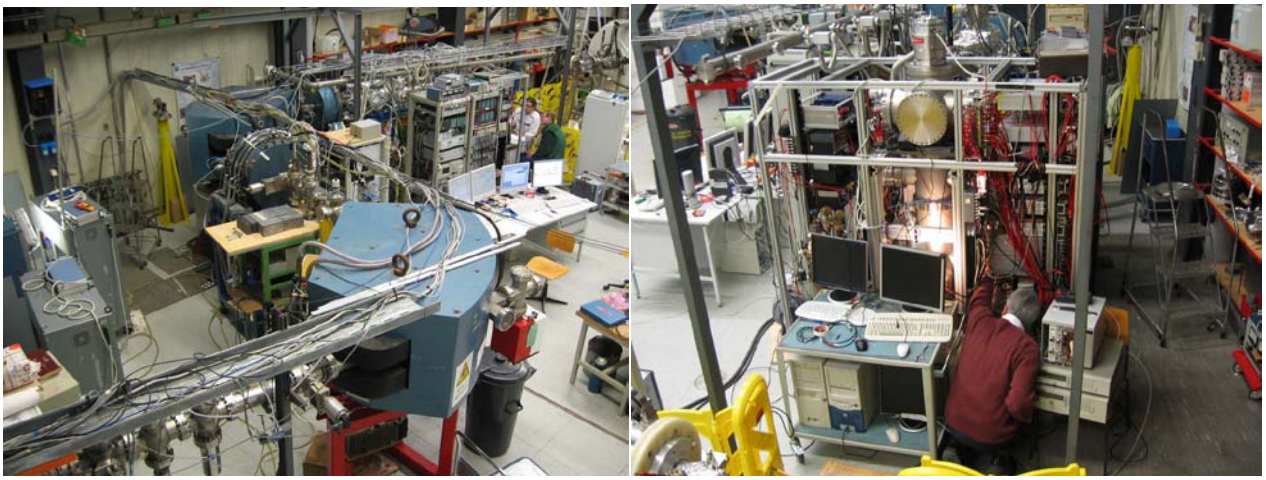

Fig. 8: Left: Overview of the experimental area at the Garching Tandem accelerator, where the Giessen MR-TOF prototype (shown on the right-hand side) was coupled to the buffer gas stopping cell.

Development of a 'detector trap' for In-Trap decay spectroscopy

Presently the quality of high-resolution electron spectroscopy is limited due to scattering and energy loss in the source material. In contrast to that a well-localized ion cloud in a Penning trap can be considered as an ideal carrier-free source for the investigation of radioactive decays, where energy loss and scattering in the carrier material are inherently avoided and thus do not influence the resulting lineshape. Moreover, isobarically pure sources can be realized in the purification trap. Simultaneously the magnetic field of the Penning trap can be exploited to guide electrons with high efficiency to detectors located outside the magnetic field. Therefore R&D is pursued at MLLTRAP to develop the technology of In-trap decay spectroscopy, combining capabilities of charged particle detection in the trap following e.g. α decay in the trap center with position-sensitive electron detection behind the trap or high-resolution electron spectroscopy. In a Penning trap a very cold ion ensemble can be prepared well-localized in the trap center with cyclotron radii typically of the order of 50 μm. The variety of physics topics that can be addressed ranges from studies of rare ground-state α decays and α decays from (high-spin) isomeric states over in-trap electron spectroscopy for the investigation of conversion electron, Auger or β decays of radioactive ion species to studies of 'shake-off' electron decays.

Typically the α decay of a heavy even-even nucleus leads with a probability of 10% - 20% to the first excited 2^+ state of the daughter nucleus [7]. The populating α decay initiates the emission of low-energy 'shake-off' electrons that allow to determine the location of the decay. After the lifetime of the 2^+ state (typically ~100 ps) it decays via L conversion, again emitting numerous shake-off electrons. During the lifetime of the 2^+ state the recoil nucleus travels a distance of typically about 50 μm, accordingly the point of origin of the shake-off electrons at the position of the conversion electron decay is displaced by this distance from the position of the α decay. This decay length can thus be measured via a measurement of the position difference of two electron peaks, one originating from the shake-off from outer electrons during the α decay, while the second peak results from those low-energy electrons emitted during the converted decay of the 2^+ state. This allows for a lifetime measurement of the 2^+ state using the 'Recoil Distance' method and hence to derive the nuclear quadrupole moment. Via a measurement of the direction of

the α decay the momentum vector of the heavy recoil nucleus can be derived. For the detection of the α decay particles a cubic arrangement of silicon strip detectors surrounding the trap center will be used that simultaneously acts as trap ring electrode. This 'Detector Trap' allows to determine the emission direction of the recoil nuclei, since the highly charged recoil nucleus will carry the same momentum as the α particle, however exhibiting a bending radius in the magnetic field reduced by the corresponding ratio of the charge states. Using an arrangement with Silicon strip detectors of 30 mm length and a strip width of 1 mm placed in a radial distance of 15 mm around the trap center will allow for a solid angle coverage of 67% of 4π. With the radial position resolution of the α detection given by the detector segmentation of 1 mm, the flight distance travelled by the recoil nucleus can be determined to an accuracy of about 3%. The low-energy conversion and shake-off electrons will be attached to the field lines of the strong trap magnetic field with small gyration radii (~ 15 μm for 1 keV electrons in a 7 T magnetic field) and can be guided with high efficiency to electron detectors at both ends of the trap, thus enabling electron -electron coincidence measurements and allowing for a precise localization of the ion cloud. A way to achieve the position-sensitive electron detection is to exploit the adiabatic expansion of the magnetic field along the trap axis, resulting in an optical magnification of the position difference of the two decays in the trap/source center, thus significantly enhancing the spatial resolution for decays of the source nuclei. A field expansion from 7 T in the trap center to e.g. ~$7{\cdot}10^{-3}$ T in about 1 m distance results in a magnification by about a factor of 30, which in turn allows to detect the position centroids of the electrons, originally only about 50 μm apart, now separated by 1.5 mm on the electron detector. Using pixelated detectors a position resolution of 0.1 mm can be achieved, resulting in an uncertainty of ≤7% for the determination of the distance between the electron cloud centroids. Altogether this results in an achievable accuracy for the lifetime measurement of the decaying 2^+ state of≤ 10%. A schematical figure of the corresponding experimental setup as proposed for the lifetime measurements at MLLTRAP is shown in Fig. 9.

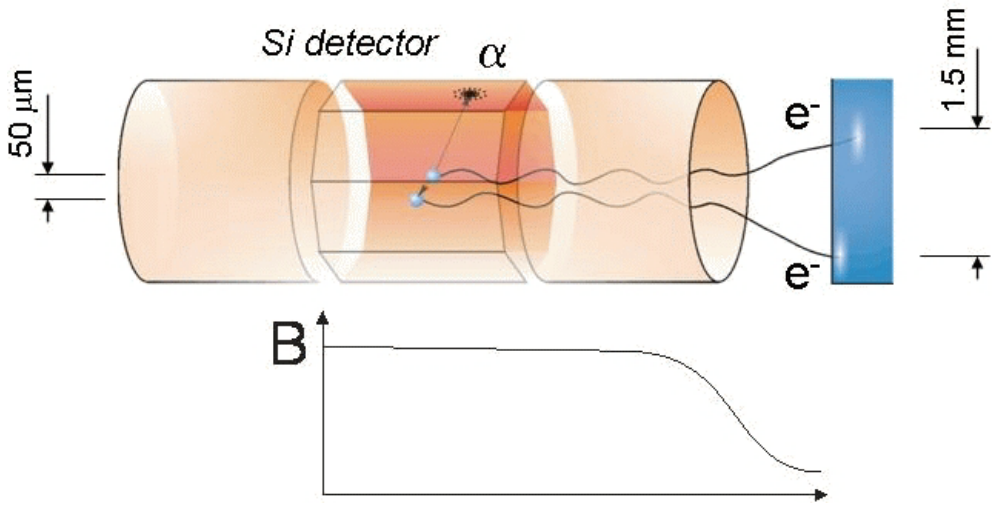

Fig.9: Schematical illustration of the proposed setup of a 'detector trap' for coincident in-trap α and electron spectroscopy aiming at the measurement of nuclear lifetimes of 2^+ states via a measurement of the flight distance between the position of the populating α decay and the subsequent conversion decay. The α decay will be measured in a cubic structure of silicon strip detectors, acting simultaneously as ring electrode of a cylindrical Penning trap, while conversion and 'shake-off' electrons will be guided by the magnetic field to electron detectors at the exit of the trap magnet.

Fig. 10 displays a design sketch of the described ‘detector trap’ in the context of the complete arrangement of the MLLTRAP double Penning trap electrodes (left part) and (right part) a front view of the cubic detector arrangement mounted inside the beam tube within the trap magnet bore.

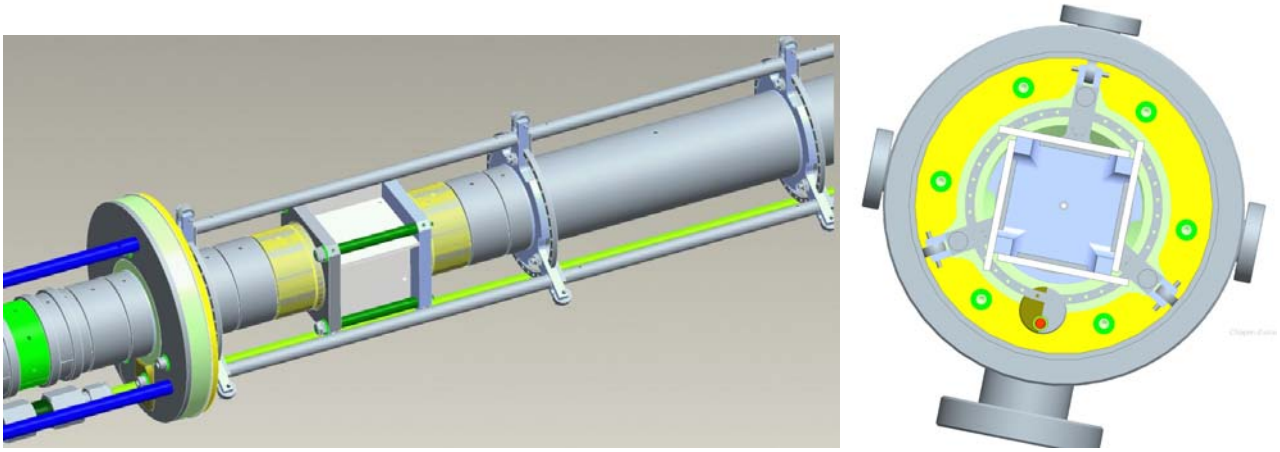

Fig. 10: Design sketch of the cubic detector trap setup replacing the cylindrical Penning trap ring electrode of the measurement trap (left part). Right side: front view of the cubic strip detector arrangement mounted inside the beam tube inside the magnet bore.

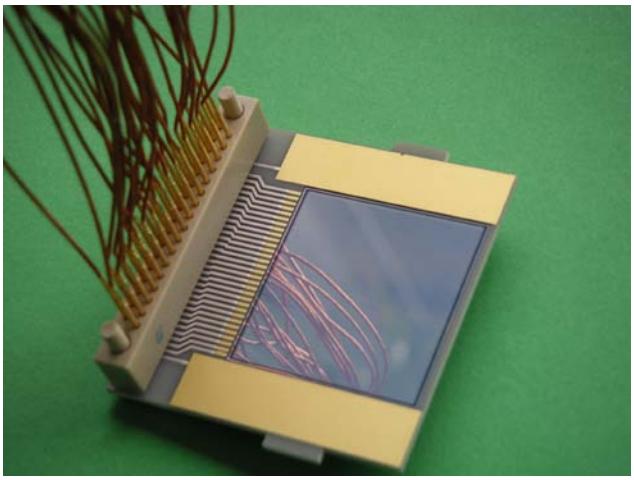

Fig. 11: Customized Si strip detector bonded to a specifically developed (AlN) ceramic board and contacted by a matched customized PEEK connector with telescope spring contacts.

Customized Si strip diodes have been developed together with a Russian manufacturer and UHV- as well as cryo-compatible ceramic (AlN) carrier boards and customized, compact high-density PEEK connectors have been developed and manufactured. Work is ongoing to commission the detectors in the laboratory as well as under magnetic field conditions. An independent and optimized trap electrode system, allowing for a fast exchange between the mass measurement and in-trap setups is under construction.

Development of a ‘Multi-Passage Spectrometer’

Further work at the MLLTRAP facility includes the setup of a 'Multi-Passage Spectrometer', i.e. a dipole magnet with round pole tips allowing for pulsed operation in combination with an electrostatic lens and mirror system, which can serve as a 4-way

beam bender as well as (q/A)-separator when using a charge breeding device aiming at the use of highly charged ions in the trap. First experimental studies at MLLTRAP aim at investigating α recoil products of actinides (e.g. ^{240}U), which are produced in high charge states. Using highly-charged ions in the Penning trap allows for a significant improvement of the mass accuracy, or, alternatively, the use of shorter measurement times for short-lived exotic species. Since any charge-breeding technique requires a subsequent q/A separator to select the charge state of interest, a 'Multi-Passage-Spectrometer' based on a dipole magnet with round pole tips is under construction at MLLTRAP. In order to allow for a fast ramping of the magnet, thus enabling a rapid variation of its bending power between injection of singly-charged and extraction of highly-charged ions, a laminated magnet yoke has been chosen. Together with a customized power supply, periodic ramping of the magnet can be performed within 50 ms, suitable also for short-lived ion species. Fig. 12 displays a schematical view (based on a design developed in [9]) of the interior of the dipole magnet vacuum chamber, housing the ion-optical lens and mirror system.

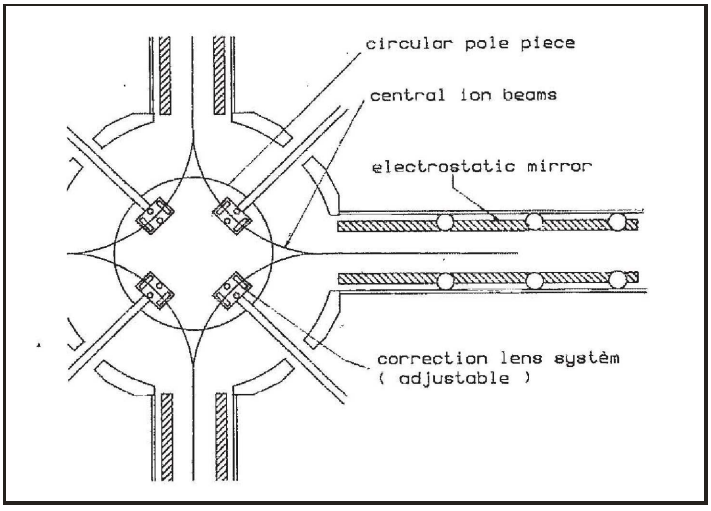

Fig. 12: Schematics of the MPS magnet chamber housing ion-optical lens and mirrors systems [9]

In order to assure a high transmission through the MPS, the magnetic field of the dipole magnet has to be known with high accuracy. Therefore a 3-axis scanning robot was constructed for an automated mapping of the magnetic field on a 1 mm grid in 3D, using a Hall probe with a positioning accuracy of <0.5 mm in each direction [8] and controlled by a LabView based control and measurement software package. Based on the resulting field map with more than 1.2 million data points (part of the field map shown in Fig. 13), ion-optical trajectory simulations for the design of deflectors and correction lenses inside the magnetic field are in progress.

Fig. 13: Photograph of the fast-ramping dipole magnet designed for the ‘Multi-Passage Spectrometer (MPS)’ to be used as q/A-separator at MLLTRAP. The right pat shows the automatic scanning device set up to map the magnetic field in 3D with mm accuracy.

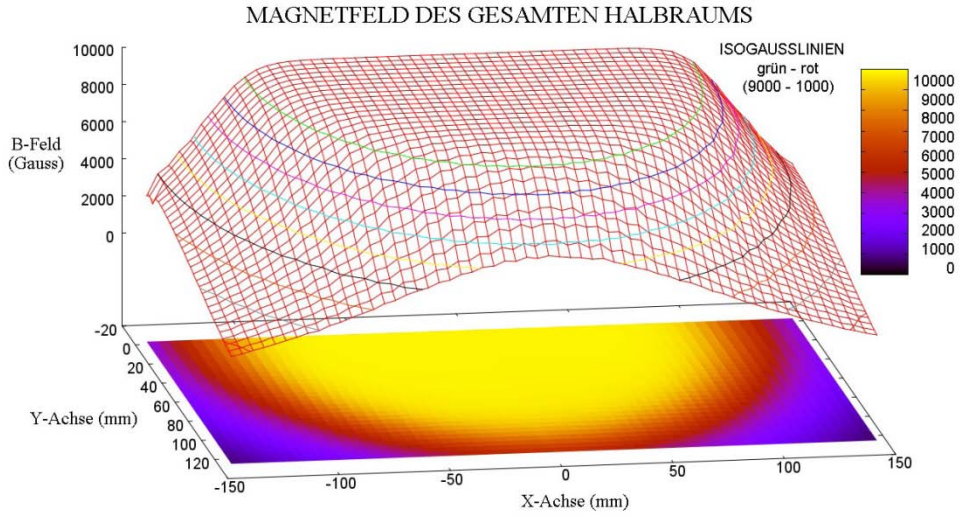

Fig. 13: Magnetic field map of the MPS dipole magnet as determined by the automatic scanning procedure described above [8].

References:

[1] V. Kolhinen et al., Nucl. Instr. and Meth. B 266, 4547 (2008).
[2] E. Gartzke, Diploma Thesis, LMU Munich (2009).
[3] K. Krug, Diploma Thesis, LMU Munich (2010).
[4] C. Droese, Diploma Thesis, Ernst-Moritz-Arndt-University Greifswald (2010).
[5] J. Neumayr et al., Rev. Sci. Instr. 77, 065109 (2006).
[6] W. Plass et al., Nucl. Instr. Meth. B 266 (2008) 4560.
[7] A. Sobiczewski et al., Phys. Rev. C 63, 034306 (2001).
[8] R. Meissner, Bachelor Thesis, LMU Munich (2011).
[9] A. Lakatos, Diploma Thesis, Univ. Frankfurt (1992).

APPENDIX 4

DESIR Collaboration Agreement DECA

DESIR

Désintégration, excitation et stockage d'ions radioactifs
Decay, excitation and storage of radioactive nuclei

Collaboration Agreement

1. Introduction

DESIR is a collaborative European project (hereafter referred to as the "Project") to construct and operate the DESIR facility at SPIRAL2 of GANIL. The DESIR facility is constituted of the RFQ cooler SHIRaC, the high-resolution separator HRS, the beam lines from the different SPIRAL1/2 production sites including from S3, and the DESIR hall. DESIR will allow for a large variety of experiments at ISOL energies to be performed.

2. Purpose of this DECA

The purpose of this DECA is to specify what the members of the DESIR collaboration intend with respect to funding, and operating experimental equipment of the DESIR facility. This instrumentation is roughly grouped in three different domains: i) studies concerning beta decay are grouped together in the BESTIOL facility, laser spectroscopy experiments in the LUMIERE facility and experiments with traps in the DETRAP facility.

The (radioactive) beams will be delivered by GANIL-SPIRAL2 operators. GANIL will be in charge of safety and security issues associated to the use of the beams and of the equipment. If the equipment does not fulfil the security and safety requirements expressed by GANIL, the later party can veto the installation and the use of the equipment. GANIL will help the users to install their equipment and to use them in optimal conditions.

This DECA is the non-binding expression of the current intentions of the Parties. None of the Parties will be bound by any legal obligation to the other Parties or incur any associated expense.

The intention of the Parties is to provide the necessary capital and human resources to successfully carry out this project.

The items forming the DESIR facility, their costing, the sharing of the required capital investment and human resources, and the installation schedule foreseen and the milestones for the Project are given in Annexe B.

Any changes in the scope of the DESIR facility will be agreed upon at the DESIR steering committee, as described in Annexe C.

The DESIR facility is sited at GANIL/SPIRAL2 (Caen, France).

3. Parties of this DECA

This DESIR Collaboration Agreement (hereinafter “DECA”) is between the Parties to this DECA (hereinafter “the Parties”). These Parties are listed in Annexe A.1. They form the DESIR Collaboration during the construction and installation phases to which this DECA applies.

4. Commencement, Duration, Withdrawal and Extension of the DECA

This DECA will become effective when at least three Parties have signed including GANIL/SPIRAL2.

This DECA shall stay in force until 31 December 2015, which is the expected end of the construction phase of DESIR. This DECA may be extended only by an amendment to the DECA.

Any Party may withdraw from the DECA by giving not less than twelve months notice in writing to the DESIR Steering Committee. It is expected that general equipment as defined in Annexe B1 and provided by the Party will remain with DESIR for the period of this DECA.

5. Organisation and Management

The DESIR organisation and the governance bodies for the construction of DESIR are described in Annexe C.

DESIR is an open collaboration. New members may accede to this DECA through a written procedure defined by the DESIR Steering Committee.

6. Amendments and Modification of the DECA

This DECA may be amended or modified at any time in writing, if agreed by at least two thirds of the Parties. This procedure is also applied, when new parties want to join this DECA.

7. General Provisions

The Parties will conduct the collaboration in terms of this DECA in compliance with the applicable laws and regulations. The obligations of each Party are subject to the availability of appropriate funds and human resources.

Nothing in this DECA will affect any other agreement concerning cooperation between the Parties.

All questions regarding the interpretation of this DECA will be resolved consensually by the Parties. Any dispute that may arise between the Parties in connection with this DECA, which cannot be resolved amicably between the Parties, shall be finally settled by the Rules of Conciliation and Arbitration of the International Chamber of Commerce by three arbitrators

appointed in accordance with the said Rules, unless the Parties agree on a single arbitrator. The award of the arbitrator will be final and binding upon the Parties concerned. Proceedings shall be conducted in English.

Information provided by any Party under this DECA and implementing agreements shall be accurate to the best of that Party's knowledge and belief, but no warranty, expressed or implied, is given by that Party to such information.

Each Party takes charge of the insurance coverage for its own staff in accordance with applicable legal requirements for occupational injuries and occupational diseases. Consequently, each party must fulfil the required formalities and sustain all the costs, if any, involved in the insurances underwritten to cover its own staff against the risks.

Each Party is liable, in accordance with the applicable law, for damages caused by its staff to the staff of any other Party.

Each Party will bear the liability without any right of claim against any other Party, except in cases of gross negligence or wilful misconduct, for any damage to its own properties resulting from or in the course of fulfilment of this DECA.

Each Party remains liable, in accordance with the applicable legal regulations, for damages caused by itself or its staff to third Parties occurring under this DECA.

8. Technical Provisions

The equipment at the DESIR facility is divided into:
(i) Experiment equipment, which will be the responsibility of individual groups, and (ii) common equipment, which the Collaboration has agreed to provide at its common expense. The former stays a property of the individual groups, whereas the latter becomes a general equipment of DESIR (see Annexe B1).

All equipment brought to *DESIR* shall comply with GANIL's safety and security regulations. The design, test criteria and testing of equipment should be discussed well in advance with GANIL's safety and security officials. All equipment brought to DESIR shall be accessible for inspection by the DESIR Technical Coordinator and by the GANIL safety and security officials at any time.

Floor space allocation for the experiments shall be co-ordinated by the DESIR Project Manager.

The following documents and annexes are an integral part of this DECA:

Annexe A:	List of Parties
Annexe B:	DESIR Equipment, Capital Investment and Installation
Annexe C:	DESIR Management Structure

This DECA is drawn up and executed in English, in one original document.

Dr. Florent Staley
Director of Grand Accélérateur National d'Ions Lourds, Caen

Pr. Philippe Moretto
Director of Centre d'Etudes Nucléaires de Bordeaux-Gradignan, Université Bordeaux I and CNRS/IN2P3

Dr. Gabriel Chardin
Director of Centre de Spectrométrie Nucléaire et de Spectrométrie de Masse Université Paris Sud and CNRS/IN2P3

Dr. Christelle Roy
Director of Institut Pluridisciplinaire Hubert Curien Université Strasbourg and CNRS/IN2P3

Dr. Fayçal Azaiez
Director of Institut de Physique Nucléaire d'Orsay, Université Paris Sud and CNRS/IN2P3

Dr. Dominique Durand
Director of Laboratoire de Physique Corpusculaire de Caen ENSICAEN, Université Caen Basse Normandie and CNRS/IN2P3

Priv. Doz. Dr. Peter G. Thirolf
Head of Nuclear Science Group
LMU Munich

Dr. Guillermo Mena Marugan
Director del Instituto de Estructura de la Materia, CSIC Madrid

Pr. Gerda Neyens
Head of the Nuclear Moments Group
K.U. Leuven

Pr. Jon Billowes
Head of Nuclear Physics Group
University of Manchester

Pr. Victor Matveev
Director JINR
Dubna

Pr. Francisco Botella Olcina
Director IFIC
CSIC & University of Valencia

Dr. Cayetano López Martínez
Director General
CIEMAT Madrid

Pr. Francisco Calvino Tavares
Nuclear Engineering Section
UPC Barcelona

Annexe A: List of Parties

- GANIL/SPIRAL2, CEA-DSM/CNRS-IN2P3
- CEN Bordeaux-Gradignan, CNRS-IN2P3/Université de Bordeaux 1
- CSNSM Orsay, CNRS-IN2P3/Université Paris 11
- IPHC Strasbourg, CNRS-IN2P3/Université de Strasbourg
- IPN Orsay, CNRS-IN2P3/Université Paris 11
- LPC Caen, CNRS-IN2P3/Université de Basse-Normandie, ENSICAEN
- LMU München
- Instituto de Estructura de la Materia IEM-CSIC Madrid
- K.U. Leuven
- University of Manchester
- FLNR JINR Dubna
- Instituto de Física Corpuscular IFIC-CSIC Valencia
- CIEMAT Madrid
- UPC Barcelona

Annexe B: DESIR Equipment, Capital Investment and Installation

Annexe B.1: DESIR Equipment and Capital Investment

Specifications of all items will be produced by the DESIR management prior to production. All cost estimates are based on 2011 prices in Euro without tax.

Definition of equipment:

General DESIR equipment (laboratory responsible):

- RFQ cooler SHIRaC (LPC Caen)
- High-resolution separator HRS (CEN Bordeaux-Gradignan)
- DESIR beam lines (IPN Orsay)
- Stable ion sources (CEN Bordeaux-Gradignan)
- General purpose ion buncher GPIB (CSNSM Orsay)
- DESIR identification station (IPHC Strasbourg)

Experiment equipment to be used at DESIR:

- Laser spectroscopy setup LUMIERE (IPN Orsay, K.U. Leuven, U. Manchester)
- The BESTIOL facility
  - Total absorption gamma-ray spectrometer TAGS (IFIC Valencia)
  - BESTIOL double Penning-trap PIPERADE (CEN Bordeaux-Gradignan)
  - Neutron ToF detector (LPC Caen, CIEMAT Madrid)
  - Charged particle array Silicon cube (CSIC Madrid, CEN Bordeaux-Gradignan)
  - Beta-decay station BEDO (IPN Orsay)
  - Neutron detector BELEN (U. Barcelona)
  - Neutron multiplicity detector TETRA (FLNR JINR Dubna)
- The DETRAP facility
  - MLL Penning trap (LMU Munich)
  - LPC Paul trap (LPC Caen)

Cost for general DESIR items:

• RFQ cooler SHIRaC:	400 k€
• High-resolution separator HRS	2000 k€
• DESIR beam lines	3960 k€
• Remote control of beam lines equipments	1500 k€
• DESIR hall	7342 k€
• Radioprotection Laboratory	87 k€
• Workshops equipment	57 k€
• Stable ion sources	59 k€
• General purpose ion buncher GPIB	390 k€
• DESIR identification station	209 k€

Cost for DESIR experiments:

- Laser spectroscopy setup LUMIERE 1000 k€
- Total absorption gamma-ray spectrometer TAGS 340 k€
- DESIR double Penning-trap PIPERADE 844 k€
- Neutron ToF detector 580 k€
- Charged particle array Silicon cube 240 k€
- Beta-decay station BEDO 250 k€
- MLL Penning trap 700 k€
- LPC Paul trap 500 k€
- Neutron detector BELEN 150 k€
- Neutron multiplicity detector TETRA 300 k€

Annexe B.2 Sharing of Capital investment and Human resources

The Parties are planning to make bids to contribute with the capital given in table B.2.1, as given in annexe B.1. In-kind contributions will be made, whenever possible, allowing making best use of the expertise and experience acquired during the R&D phase. The first three DESIR items (RFQ cooler SHIRaC, the HRS, the beam lines) are not included, as they will be financed by different means (CPER, EQUIPEX). For some of the equipment, the full amount mentioned in table B.1 is not yet reached in table B2.1. For this equipment, the numbers in table B2.1 correspond to phase 1 of the full project.

The Parties are planning to make human resources (physicists, engineers and technicians) as given in table B.2.1 available to the *DESIR* project (personnel in person-months).

Table B.2.1 Capital investment and human resources committed for the DESIR R&D and installation phase.

Party	Planned capital investment (k€)	Funds committed (k€)	Personnel in person months
EU	0	241	0
GANIL Caen	0	0	53.4
CENBG Bordeaux	0	657	200
IPHC Strasbourg	209	0	24.1
LPC Caen (LPCTrap)	200	300	10
LPC Caen (Neutron-TOF)	235	45	15
CSNSM Orsay	0	187	76
IPN Orsay (LASER)	137	177	0
IPN Orsay (BEDO)	250	0	40
LMU Munich	0	700	18
University of Manchester	150	70	12
KU Leuven	200	100	12
IFIC-CSIC Valencia	0	340	10
IEM-CSIC Madrid	0	240	10
CIEMAT Madrid	0	300	10
UPC Barcelona	0	150	12
FLNR JINR Dubna	200	100	16
Total	**1 381**	**3 727**	**518.5**

Annexe B.3: Construction schedule and Milestones

Provisional planning and milestones for the construction and installation of the DESIR facility.

Month/year	Item
05/2014	completion of the DESIR beam line tunnels
06/2014	installation of beam lines
06/2014	completion of the DESIR hall
07/2014	installation of the general purpose equipment
03/2015	installation of parts of the BESTIOL equipment
07/2015	completion of the LPC Paul trap
09/2015	completion of the MLL trap in DESIR
12/2015	completion of phase 1 of the LUMIERE facility
12/2015	completion of beam lines

Annexe C:

DECA Management Structure

The organisation for the construction and the commissioning of the DESIR experimental equipments comprises the following bodies:

- The DESIR Steering Committee, acting on behalf of the Parties, is responsible for the Project coordination and the science policy of the collaboration.
- The DESIR Collaboration Council, representing all Parties under the DESIR project, advises the DESIR Steering Committee on scientific matters.
- The DESIR Management Board is responsible for the execution of the Project along the lines defined by the DESIR Steering Committee.

The terms of reference of each of these bodies is given in more detail below.

DESIR Steering Committee

Membership:
Members are nominated by the Parties of the DECA. Each party will have one member.

The DESIR Spokesperson attends meetings for consultation only and therefore without voting rights. The DESIR Steering Committee can invite others to attend as needed for consultation only, for example the DESIR Facility Coordinator.

Voting rights:
All members have equal voting rights. The GANIL representative has a veto right in case equipment does not comply with GANIL security and safety rules.

Terms of reference:
The DESIR Steering Committee is the decision-making body of the DESIR Collaboration and responsible for the allocation of resources supplied by the Parties. The DESIR Steering Committee, in agreement with the scientific bodies of GANIL, will ensure that the primary criterion for deployment of any equipment is based on scientific merit and obey the GANIL safety and security rules.

The tasks of the Steering Committee are as follows:

1. Define the scientific policy of the DESIR Collaboration taking advice from the DESIR Collaboration Council.
2. Elect a chair and vice-chair among its members who will each serve for a period of two years.
3. Appoint members of the DESIR Management Board.
4. Monitor the Project based on reports received from the DESIR Spokesperson.
5. Decide on any modification of the Project proposed by the DESIR Spokesperson.
6. Review the progress of the DESIR project based on reports received from the DESIR Spokesperson.

7. Review the cost statements and allocations.

Decisions in the DESIR Steering Committee shall be taken by consensus.

The DESIR Steering Committee shall not make any decision unless a quorum of two thirds of the members are represented.

Minutes of each meeting shall be drafted by the chairperson to the other members without delay. The minutes of each meeting shall be considered as accepted by the other members if, within thirty calendar days from receipt, the other members have not objected in writing to the chairperson.

The DESIR Steering Committee chair signs on behalf of the DESIR Steering Committee all written agreements.

DESIR Collaboration Council

Membership:
One representative from each Party, the DESIR Spokesperson and the DESIR facility coordinator. The DESIR Spokesperson chairs the meetings of the DESIR Collaboration Council.

Voting:
All members have equal voting rights. The DESIR Spokesperson is excluded from any vote concerning the Spokesperson's role.

Terms of Reference:
The DESIR Collaboration Council is the advisory body of the DESIR Steering Committee on scientific matters concerning the DESIR facility.

The tasks of the DESIR Collaboration Council are as follows:

1. Elect the DESIR Spokesperson who will serve for a period of two years.
2. Advise the DESIR Steering Committee on scientific matters concerning the DESIR facility and the research programme through the DESIR Spokesperson.
3. Hold meetings, at least annually, to receive reports from the DESIR Steering Committee and DESIR Management Board on the progress of DESIR and from the DESIR Spokesperson on the progress of the installation programme.
4. Hold an annual open meeting of the DESIR collaboration to present the status of DESIR and to discuss future evolutions.

DESIR Management Board

Membership of the DESIR Management Board:
The DESIR Spokesperson, the DESIR Facility Coordinator, chairpersons of the major setups at DESIR (LUMIERE, BESTIOL, DETRAP), chairperson of the DESIR Steering Committee (ex-officio). The DESIR Spokesperson will chair the DESIR Management Board meetings.

Voting rights:
All members have equal voting rights.

Terms of Reference:
The DESIR Management Board runs the DESIR facility. The DESIR Management Board shall report to and be accountable to the DESIR Steering Committee through the DESIR Spokesperson.

The tasks of the DESIR Management Board are as follows:

1. Supervise the effective and efficient installation of the facility.
2. Collect information on the progress of DESIR, examine that information to assess the compliance of the Project with the programme decided by the DESIR Steering Committee and, if necessary, propose modifications of the programme to the DESIR Steering Committee.
3. Provide reports of the progress of DESIR to the DESIR Steering Committee including an annular planning and resource report.
4. Advise the DESIR Steering Committee on technical issues.
5. Work with the spokespersons of the DESIR equipment or equipment installed in DESIR to ensure the successful operation of DESIR.
6. Organise DESIR working group meetings as needed.

DESIR Spokesperson

The DESIR Spokesperson is elected by the DESIR Collaboration Council to coordinate the DESIR collaboration. For this purpose the Spokesperson can create and dissolve working groups as needed and after acceptance of the DESIR Steering Committee. The Spokesperson will nominate the chairpersons of these working groups.

DESIR Facility Coordinator

The DESIR Facility Coordinator is nominated by GANIL. He supervises all technical issues of the DESIR facility on a daily basis. He/She regularly reports to the DESIR Spokesperson. The DESIR Facility Coordinator is a full member of the DESIR Management Board and of the DESIR Collaboration Council.

Annexe D:

Experiment equipment to be used at DESIR

1. Group of Instituto de Estructura de la Materia, IEM-CSIC, Madrid

The contribution consists in setting up a line for general purpose beta decay studies.

Vacuum:			
Vacuum chamber		15.000	
Pumps and control		25.000	40.000
Silicon:			
Telescope=DSSSD + PAD		10.000 x6	60.000
Electronics 200 channels x 150 €		30.000	90.000
Gamma:			
CEPA phoswich LABrLaCL Array			60.000
Digitizer		10.000	70.000
DAQ:			
VME	5.000		
CPU	5.000		
NIM-logic	10.000		
TDC	10.000		
Scaler	10.000		40.000
			==========
TOTAL			**240.000**

2. Equipment from Instituto de Fisica Corpuscular, IFIC-CSIC, Valencia

The equipment comprises a total absorption gamma-ray spectrometer for beta-decay studies and the associated electronics and data acquisition system.

Item	**Cost (in euro)**
BaF_2 12-fold segmented spectrometer	185000
Electronics for spectrometer	37800
Ancillary detectors (plastic, Si, HPGE)	22000
Electronics for ancillary detectors	17800
Trigger electronics	20900
Data acquisition system	39500
Lead shielding	12000
Mechanical support	5000
	==========
TOTAL	**340000**

3. Equipment from the Centro de Investigaciones Energéticas, Medioambientales y Tecnológicas, CIEMAT, Madrid

The equipment comprises a neutron spectrometer made of 30 liquid scintillator cells for beta-decay studies, electronics and mechanical structure.

Item	**Cost (in euro)**
30 cells of BC501A	180000
30 Hamamatsu R4144 photomultipliers	60000
Electronics for the spectrometer	30000
Data acquisition system	60000
Mechanical support	10000
	==========
TOTAL	**340000**